



# Observation and modelling of OH and HO<sub>2</sub> concentrations in the Pearl River Delta 2006: a missing OH source in a VOC rich atmosphere

K. D. Lu<sup>1,2</sup>, F. Rohrer<sup>2</sup>, F. Holland<sup>2</sup>, H. Fuchs<sup>2</sup>, B. Bohn<sup>2</sup>, T. Brauers<sup>2</sup>, C. C. Chang<sup>3</sup>, R. Häseler<sup>2</sup>, M. Hu<sup>1</sup>, K. Kita<sup>4</sup>, Y. Kondo<sup>5</sup>, X. Li<sup>1,2</sup>, S. R. Lou<sup>2,6,\*</sup>, S. Nehr<sup>2</sup>, M. Shao<sup>1</sup>, L. M. Zeng<sup>1</sup>, A. Wahner<sup>2</sup>, Y. H. Zhang<sup>1</sup>, and A. Hofzumahaus<sup>2</sup>

<sup>1</sup>College of Environmental Sciences and Engineering, Peking University, Beijing, China

<sup>2</sup>Institut für Energie und Klimaforschung: Troposphäre, Forschungszentrum Jülich, Jülich, Germany

<sup>3</sup>Research Center for Environmental Changes, Academic Sinica, Taipei, China

<sup>4</sup>Faculty of Science, Ibaraki University, Ibaraki, Japan

<sup>5</sup>University of Tokyo, Research Center for Advanced Science and Technology, Tokyo, Japan

<sup>6</sup>School of Environmental Science and Technology, Shanghai Jiao Tong University, Shanghai, China

\* now at: Shanghai Academy Of Environmental Sciences, Shanghai, China

Correspondence to: A. Hofzumahaus (a.hofzumahaus@fz-juelich.de), Y. H. Zhang (yhzhang@pku.edu.cn)

Received: 28 March 2011 – Published in Atmos. Chem. Phys. Discuss.: 12 April 2011

Revised: 10 January 2012 – Accepted: 30 January 2012 – Published: 9 February 2012

**Abstract.** Ambient OH and HO<sub>2</sub> concentrations were measured by laser induced fluorescence (LIF) during the PRIDE-PRD2006 (Program of Regional Integrated Experiments of Air Quality over the Pearl River Delta, 2006) campaign at a rural site downwind of the megacity of Guangzhou in Southern China. The observed OH concentrations reached daily peak values of  $(15\text{--}26) \times 10^6 \text{ cm}^{-3}$  which are among the highest values so far reported for urban and suburban areas. The observed OH shows a consistent high correlation with  $j(\text{O}^1\text{D})$  over a broad range of NO<sub>x</sub> conditions. The correlation cannot be reproduced by model simulations, indicating that OH stabilizing processes are missing in current models. The observed OH exhibited a weak dependence on NO<sub>x</sub> in contrast to model predictions. While modelled and measured OH agree well at NO mixing ratios above 1 ppb, a continuously increasing underprediction of the observed OH is found towards lower NO concentrations, reaching a factor of 8 at 0.02 ppb NO. A dependence of the modelled-to-measured OH ratio on isoprene cannot be concluded from the PRD data. However, the magnitude of the ratio fits into the isoprene dependent trend that was reported from other campaigns in forested regions. Hofzumahaus et al. (2009) proposed an unknown OH recycling process without NO, in order to explain the high OH levels at PRD in the presence of high VOC reactivity and low NO. Taking a recently discovered interference in the LIF measurement of HO<sub>2</sub> into ac-

count, the need for an additional HO<sub>2</sub> → OH recycling process persists, but the required source strength may be up to 20 % larger than previously determined. Recently postulated isoprene mechanisms by Lelieveld et al. (2008) and Peeters and Müller (2010) lead to significant enhancements of OH expected for PRD, but an underprediction of the observed OH by a factor of two remains at low NO (0.1–0.2 ppb). If the photolysis of hydroperoxy aldehydes from isoprene is as efficient as proposed by Peeters and Müller (2010), the corresponding OH formation at PRD would be more important than the primary OH production from ozone and HONO. While the new isoprene mechanisms need to be confirmed by laboratory experiments, there is probably need for other, so far unidentified chemical processes to explain entirely the high OH levels observed in Southern China.

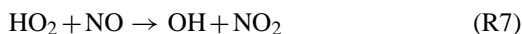
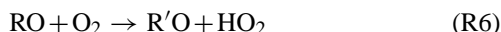
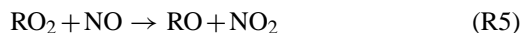
## 1 Introduction

Hydroxyl (OH) and peroxy (HO<sub>2</sub>, RO<sub>2</sub>) radicals play an essential role in atmospheric chemistry on local to global scales (e.g. Brasseur et al., 2003; Monks et al., 2009). Reactions with the most important atmospheric oxidant, OH, initiate the chemical breakdown of tropospheric trace gases such as CO, SO<sub>2</sub>, NO<sub>2</sub>, CH<sub>4</sub> and other volatile organic compounds (VOCs). Many of these reactions produce HO<sub>2</sub> and RO<sub>2</sub>,

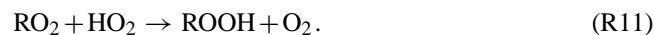
which are key intermediates in the formation of secondary, atmospheric pollutants (Finlayson-Pitts and Pitts Jr., 2000). Reactions (R1)–(R4) represent examples of HO<sub>2</sub> and RO<sub>2</sub> forming reactions:



Reactions of peroxy radicals with NO constitute the exclusive pathway for tropospheric ozone formation,

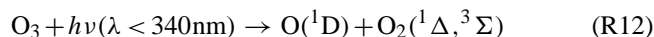


and recombination reactions of peroxy radicals represent a source of peroxides (H<sub>2</sub>O<sub>2</sub>, ROOH).



Oxy radicals, RO, produced by Reaction (R5), are generally converted to oxygenated VOCs (OVOCs), either by fast reaction with O<sub>2</sub> yielding carbonyl compounds, R'O (Reaction R6), or by unimolecular decomposition and isomerization reactions (Atkinson, 1997). OVOCs are currently receiving growing attention in atmospheric chemistry. Firstly, they may contribute significantly, sometimes 50% and more to the organic reactivity in various tropospheric environments, thereby affecting the atmospheric lifetime of OH (Lou et al., 2010; Mao et al., 2010; Shao et al., 2009; Steiner et al., 2008; Emmerson et al., 2007; Yoshino et al., 2006; Lewis et al., 2005). Secondly, photolysis of OVOCs can be a significant source of radicals at urban conditions (Emmerson et al., 2007; Kanaya et al., 2007b; Volkamer et al., 2007; Dusanter et al., 2009). Thirdly, OVOCs are precursors of secondary organic aerosols (SOA) which play a distinct role for air quality and climate (e.g. Hallquist et al., 2009; Kanakidou et al., 2005).

The atmospheric abundance of OH and HO<sub>2</sub>, collectively called HO<sub>x</sub>, depends critically on primary production processes with contributions by photolysis of ozone,



photolysis of nitrous acid and OVOCs, and O<sub>3</sub>-alkene reactions (Fig. 1). Ensuing chain reactions (Reactions R1–R7, indicated by red arrows in Fig. 1) oxidize CO, VOCs and NO, but also interconvert RO<sub>x</sub> radicals (= OH+HO<sub>2</sub>+RO<sub>2</sub>). Radical recycling by Reactions (R5)–(R7) is of particular relevance, as it constitutes a secondary source of OH which

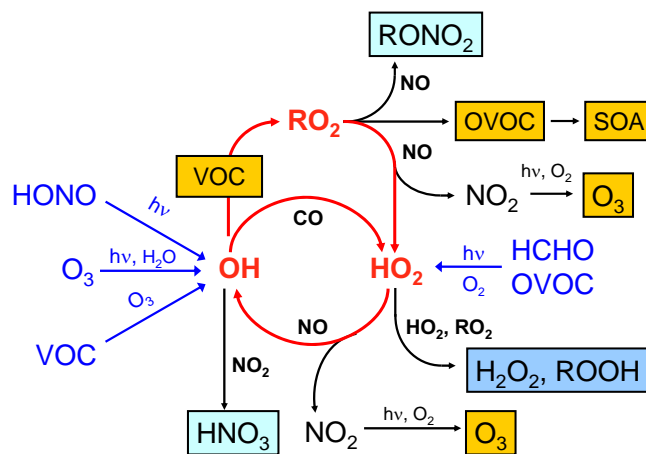
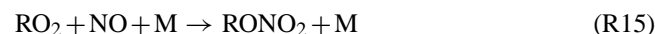


**Fig. 1.** Schematic drawing of HO<sub>x</sub> chemistry, illustrating established, major chemical pathways in the troposphere. Radical chemistry is initiated by primary radical production (blue arrows) through photodissociation and ozonolysis reactions and is terminated by radical recombination reactions forming nitric acid (HNO<sub>3</sub>), hydroperoxides (H<sub>2</sub>O<sub>2</sub>, ROOH) and organic nitrates (RONO<sub>2</sub>). Radical chain reactions (red arrows) cause cycling between OH, HO<sub>2</sub>, and RO<sub>2</sub>. Reactions of RO<sub>2</sub> and HO<sub>2</sub> with NO reproduce OH (secondary OH production) and lead to photochemical formation of ozone, OVOCs and SOA.

significantly enhances the oxidation efficiency of the troposphere (e.g. Ehhalt, 1999). Radical recombination reactions (e.g. Reactions R10, R11, R14, R15), however, cause chain termination and suppress the concentrations of OH, HO<sub>2</sub> and RO<sub>2</sub> radicals.



Highly sensitive instruments for in-situ measurement of HO<sub>x</sub> became available in the 1990s (Crosley, 1995) and have been employed in an increasing number of field experiments to test atmospheric chemical mechanisms over a broad range of tropospheric conditions. Early studies were carried out mostly in clean (polar, marine) and moderately polluted (rural) regions (Heard and Pilling, 2003), whereas many recent investigations were focussed on environments with high loads of reactive trace gases (Monks et al., 2009). These include polluted cities and their urban-influenced surroundings, as well as forests with high concentrations of biogenic VOCs. Most urban studies have shown reasonable agreement between modelled and measured OH within a factor of two when VOCs and NO<sub>x</sub> were abundant (e.g. Kanaya et al., 2007b; Shirley et al., 2006; Mihelcic et al., 2003). However, current models tend to underpredict the observed OH by up to an order of magnitude at low NO<sub>x</sub>, when isoprene reaches mixing ratios of several ppb at the same time. This trend has been clearly identified in forested regions, such as in North America (Tan et al., 2001; Ren et al., 2008), over

the Amazonian rainforest (Lelieveld et al., 2008) and the tropical forest of Borneo (Pugh et al., 2010; Whalley et al., 2011). The observations suggest that as-yet-unknown recycling reactions of peroxy radicals constitute a significant OH source, when NO mixing ratios become small. This hypothesis is consistent with a budget analysis of HO<sub>x</sub> in isoprene-containing urban air near Nashville by Thornton et al. (2002), who supposed that self reactions of peroxy radicals possibly recycle OH, rather than acting as an HO<sub>x</sub> sink (Reaction R11).

The above findings from urban and forest studies are in agreement with our investigation in Southern China (Hofzumahaus et al., 2009). In summer 2006, we performed a field campaign in the densely populated Pearl River Delta (PRD), close to the megacity of Guangzhou in Guangdong province, where atmospheric conditions were strongly influenced by both urban and biogenic emissions. In this subtropical region, air quality has been deteriorating over the past two decades owing to a fast growing economy and increasing urbanization (Chan and Yao, 2008; Zhang et al., 2008). At a rural site downwind of Guangzhou, we performed the ground-based field campaign PRIDE-PRD2006 (Program of Regional Integrated Experiments of Air Quality over the Pearl River Delta, 2006), in order to study the photochemical processing of atmospheric urban pollutants (Zhang et al., 2012). During the intensive campaign, trace gases, photolysis frequencies, aerosols, and meteorological parameters were measured. The measurements included OH and HO<sub>2</sub>, as well as the total OH reactivity,  $k_{\text{OH}}$ , which is equivalent to the reciprocal atmospheric OH lifetime (Lou et al., 2010).

On most days, the local atmosphere changed from an urban-type composition with high concentrations of anthropogenic VOCs and NO<sub>x</sub> in the morning to an atmosphere with relatively low NO (0.1–0.2 ppb) and a significant biogenic contribution (≈40%) of isoprene and its oxidation products to  $k_{\text{OH}}$  in the afternoon (Lou et al., 2010). The field campaign data were used to evaluate the OH budget by comparing the experimental OH loss rate,  $k_{\text{OH}} \times [\text{OH}]$ , with the total OH production rate,  $P'_{\text{OH}}$ , of the known primary (e.g. Reaction R13) and secondary OH production (Reaction R7) processes (Hofzumahaus et al., 2009). The OH loss rate was found to be balanced by  $P'_{\text{OH}}$  in the morning, when HO<sub>2</sub> was efficiently recycled to OH by reaction with NO (1–20 ppb). However,  $P'_{\text{OH}}$  was significantly smaller (by about a factor ≈3 at noon) than  $k_{\text{OH}} \times [\text{OH}]$ , when NO decreased to values below 1 ppb around and past noon, indicating a missing OH source.

The OH budget analysis was consistent with a comparison of model and measurement results for OH and  $k_{\text{OH}}$ . For  $k_{\text{OH}}$ , agreement of measured and modelled values was obtained within 20% during the whole daytime, suggesting that the total reactivity of OH reactants was well determined at high and low NO<sub>x</sub> conditions (Lou et al., 2010). In case of OH, modelled and measured concentrations were in agreement at

high NO<sub>x</sub> in the morning, but a significant underprediction of measured OH by a factor 3–5 was found in the afternoon at low NO<sub>x</sub> (Hofzumahaus et al., 2009). The model could be matched to the afternoon OH observations by assuming additional NO-independent recycling of OH from peroxy radicals, without impairing the good agreement between model and measurement results in the morning hours. The interesting question is, whether the missing OH sources postulated for tropical forests, North American forests, and the densely-populated PRD region are mechanistically the same.

Butler et al. (2008) and Kubistin et al. (2010) introduced an artificial reaction of isoprene hydroxyperoxy radicals (ISOP) with HO<sub>2</sub> (ISOP + HO<sub>2</sub> →  $n\text{OH}$ ) into global and box models, respectively, to simulate the assumed additional OH recycling over the Amazonian rainforest. For best fit to the OH observations, OH yields of  $n = 2$  and  $n = 3.2$  were required in the respective models. In order to describe the measured data of OH and HO<sub>2</sub> at PRD, Hofzumahaus et al. (2009) implemented two hypothetical reactions (RO<sub>2</sub> + X → HO<sub>2</sub> and HO<sub>2</sub> + X → OH, both of the same rate as for the corresponding NO reactions) into a box model. An NO equivalent of 0.8 ppb was assumed for X to match the mean diurnal profiles of both HO<sub>x</sub> species.

Recent model studies have attempted to identify the actual reaction mechanisms underlying the non-classical (without NO) OH recycling in forested regions. OH regenerating reactions of HO<sub>2</sub> with acyl peroxy and β-keto peroxy radicals, known from various laboratory studies (Jenkin et al., 2010, 2007; Dillon and Crowley, 2008; Hasson et al., 2004), were found to increase modelled OH by at most 7% above tropical rainforests (Peeters and Müller, 2010; Stavrou et al., 2010; Archibald et al., 2010; Pugh et al., 2010). In addition, the OH-neutral oxidation of isoprene hydroperoxides to dihydroxy epoxides, experimentally studied by Paulot et al. (2009), has the potential to further increase the modelled OH concentration by up to 25% in the tropics, depending on the specific isoprene degradation mechanism being used (Stavrou et al., 2010; Archibald et al., 2010). However, even together the above processes are not sufficient to explain the factor-of-10 discrepancy between modelled and observed OH above the Amazonian rainforest.

Based on ab initio calculations, Peeters et al. (2009) and Peeters and Müller (2010) have postulated a new isoprene degradation mechanism (Leuven Isoprene Mechanism, LIM0) which recycles HO<sub>x</sub> with high efficiency at low NO. The new mechanism proposes a fast interconversion of isoprene hydroxyperoxy radical isomers, some of which undergo fast 1,6-H shift, followed by reaction with O<sub>2</sub>. This predominating reaction path is expected to form HO<sub>2</sub> and hydroperoxy aldehydes (HPALDs). The HPALDs are assumed to undergo photodissociation at a high photolysis rate, leading to a net formation of one HO<sub>2</sub> and up to three OH radicals. The implementation of the LIM0 mechanism increases the modelled OH concentrations for the conditions over the Amazonian rainforest by up to a factor of four, showing

potential to explain the non-classical OH recycling in regions with high isoprene emissions (Stavrakou et al., 2010; Archibald et al., 2010).

In the present work, we investigate whether the newly proposed recycling mechanisms can explain the high OH levels at PRD, where NO concentrations span a broad range (0.02–10 ppb) and where anthropogenic VOCs are present besides isoprene. First, we report experimental details of the measurements of HO<sub>x</sub> during the PRIDE-PRD2006 campaign and demonstrate the stabilizing effect of the unknown OH source on the observed OH concentration as a function of the ozone photolysis frequency,  $j(\text{O}^1\text{D})$ , and NO<sub>x</sub>. We test different recycling mechanisms to investigate their impact on atmospheric OH and HO<sub>2</sub> for the conditions at PRD. The analysis is complicated by a recently discovered interference in our HO<sub>2</sub> measurements, which are significantly biased by the detection of specific organic peroxy radicals, such as isoprene hydroxyperoxy radicals (Nehr et al., 2011; Fuchs et al., 2011). The results reported by Hofzumahaus et al. (2009) are revised, accordingly.

## 2 Methodology

### 2.1 Measurement site

The measurements presented in this paper took place alongside a drinking water reservoir in a recreation area called Guangzhou Backgarden about 60 km northwest of downtown Guangzhou on 3–30 July 2006. Backgarden is located in a slightly mountainous area at 23.487° N, 113.034° E and is surrounded by farmland, which is mainly covered by tropical shrubs and economic crops like lichees and peanuts. During the intensive campaign period, due to the Asian monsoon, the dominant wind direction was south to south east, making Backgarden a receptor site for the outflow of urban emissions from Guangzhou. However, local wind speeds were generally low (often less than 2 m s<sup>-1</sup>), which is typical for inland PRD during summer season and favors accumulation of air pollutants (Chan and Yao, 2008). During the campaign, the weather was characterized by high humidity with absolute water-vapor mixing ratios of 2.5–4 % and high temperatures of about 28–36 °C.

Besides HO<sub>x</sub> (see next section), a comprehensive set of trace gases was measured during the campaign. Table 1 gives an overview of the measured species which are relevant for this paper and specifies the measurement techniques and their performance. Further instrumental details can be found in Lou et al. (2010). The C<sub>3</sub>–C<sub>12</sub> VOCs, measured by online gas chromatography (GC), are specified in Table 2. They include alkanes, alkenes, aromatics, and isoprene. No in-situ OVOCs measurements were available; but on some days, the averaged HCHO and glyoxal concentrations for certain air masses spanning several kilometers were retrieved by MAX-DOAS (Li et al., 2012). Most trace gases were sampled at

10 m above ground on top of a building. HO<sub>x</sub>,  $k_{\text{OH}}$ , HONO and meteorological data were measured nearby (30 m distance) at 7 m height on top of two stacked sea containers. On the containers, the photolysis frequencies  $j(\text{O}^1\text{D})$  for Reaction (R12) and  $j(\text{NO}_2)$  for Reaction (R8) were measured by calibrated filterradiometers. On the nearby building,  $j(\text{O}^1\text{D})$ ,  $j(\text{NO}_2)$ ,  $j(\text{HONO})$ ,  $j(\text{HCHO})$  etc. were obtained from solar UV spectra measured by actinic-flux spectroradiometry (Bohn et al., 2008). Both sets of  $j(\text{O}^1\text{D})$  and  $j(\text{NO}_2)$  data were in agreement within 5 %. A summary of the general conditions encountered during the PRD campaign is given in Table 3, which presents mean values for the morning at 06:00–10:00 CNST and afternoon at 12:00–16:00 CNST (CNST = Chinese Standard Time = UTC + 8 h) over the days when HO<sub>x</sub> measurements are available.

### 2.2 Radical measurements

OH, HO<sub>2</sub> and  $k_{\text{OH}}$  were measured by a compact laser-induced fluorescence (LIF) system built at Forschungszentrum Jülich, Germany (Fig. 2). The technique was initially developed for measurement of OH (Holland et al., 1995, 1998; Hofzumahaus et al., 1996) and was later extended by an additional measurement capability for HO<sub>2</sub> (Holland et al., 2003). The LIF instrument used at PRD is a follow-up version of the earlier system. It is designed to be smaller and more light-weight than the previous instrument, making the instrument easier to handle in field applications (e.g. Kl-effmann et al., 2005; Schlosser et al., 2009). Furthermore, the newly developed LP-LIF (laser-flash photolysis laser-induced fluorescence) technique for measurement of  $k_{\text{OH}}$  was implemented (Lou et al., 2010) utilizing the same tunable laser source for OH detection. In the following, the LIF system for HO<sub>x</sub> detection will be described briefly, explaining the general principle and technical differences between this and the earlier instrument version.

Radicals are sampled by expansion of ambient air through an inlet nozzle (0.4 mm orifice, Beam-Dynamics) into a low pressure (3.5 mbar) chamber, where OH is detected by LIF at 308 nm. HO<sub>2</sub> is monitored in a separate parallel detection chamber, in which HO<sub>2</sub> is first chemically converted to OH by reaction with injected NO, followed by LIF detection of OH. It should be noted that the two detection cells are mechanically connected by a set of laser-baffle arms, but are separated by a quartz window preventing any possible contamination of the OH cell by NO from the HO<sub>2</sub> cell. The two detection chambers share one dry-vacuum pump (IPX500, BOC-Edwards) and are constantly purged by a background flow of pure nitrogen through the detection cell (1 slpm; slpm = litre per minute at 1 atm, 298 K) and through the baffle arms (0.2 slpm). In each detection chamber, the gas expansion produces a gas beam through the center of the cell, which is irradiated at right angle by a 308 nm laser beam (8–10 mm diameter) from a pulsed narrow-bandwidth UV laser system operated at a repetition rate of 8.5 kHz. The

**Table 1.** Instruments for atmospheric trace gas measurements at Backgarden in summer 2006.

Compound	Measurement technique	Time resolution	LOD (1 $\sigma$ )	Accuracy (1 $\sigma$ )
OH	Laser induced fluorescence	5 min	(0.5–1) $\times 10^6$ cm <sup>-3</sup>	20 %
HO <sub>2</sub> <sup>a</sup>	Chemical conversion and laser induced fluorescence	5 min	(1–3) $\times 10^6$ cm <sup>-3</sup>	(b)
O <sub>3</sub>	UV photometry	1 min	0.3 ppb	5 %
NO	Chemiluminescence	1 min	50 ppt	7 %
NO <sub>2</sub>	Photolytical converter and chemiluminescence	1 min	170 ppt	13 %
HONO	LOPAP <sup>c</sup>	5 min	7 ppt	10 %
CO	IR photometry	1 min	4 ppb	5 %
CH <sub>4</sub>	FTIR <sup>d</sup>	10 min	0.5 ppm	4 %
C <sub>2</sub> H <sub>6</sub>	Canister sample – GC <sup>e</sup>	10 s	2 ppt	5 %
C <sub>2</sub> H <sub>4</sub>	Canister sample – GC <sup>e</sup>	10 s	3 ppt	10 %
C <sub>3</sub> –C <sub>12</sub> VOCs	Online – GC <sup>e</sup>	1 h	6–70 ppt	10 %

<sup>a</sup> HO<sub>2</sub> measurement contains an uncorrected contribution by RO<sub>2</sub>; <sup>b</sup> 20 % by calibration plus contribution by RO<sub>2</sub> interference (see text); <sup>c</sup> Long-path absorption photometry; <sup>d</sup> Fourier-transform infrared spectrometry; <sup>e</sup> Gas chromatography; see measured species in Table 2

**Table 2.** Measured hydrocarbons and their assignment to RACM species.

RACM	Measured hydrocarbons
CH <sub>4</sub>	Methane
ETH	Ethane
HC3	Propane, <i>n</i> -Butane, <i>i</i> -Butane, 2,2-Dimethylbutane
HC5	<i>n</i> -Pentane, <i>i</i> -Pentane, Cyclopentane, <i>n</i> -Hexane, 2,3-Dimethylbutane, 2-Methylpentane, 3-Methylpentane, <i>n</i> -Heptane, 2,4-Dimethylpentane, 2,3-Dimethylpentane
HC8	Cyclohexane, Methylcyclopentane, 2-Methylhexane, 3-Methylhexane, Methylcyclohexane, <i>n</i> -Octane, 2-Methylheptane, 3-Methylheptane, <i>n</i> -Nonane, <i>n</i> -Decane, <i>n</i> -Undecane, <i>n</i> -Dodecane,
ETE	Ethene
OLT	Propene, 1-Butene, 1-Pentene
OLI	<i>cis</i> -2-Butene, <i>trans</i> -2-Butene, <i>cis</i> -2-Pentene, <i>trans</i> -2-Pentene
ISO	Isoprene
TOL	Benzene, Toluene, Ethylbenzene, <i>n</i> -Propylbenzene, <i>i</i> -Propylbenzene
XYL	<i>o</i> -Xylene, <i>m</i> -Xylene, <i>p</i> -Xylene, <i>o</i> -Ethyltoluene, <i>m</i> -Ethyltoluene, <i>p</i> -Ethyltoluene, Styrene, <i>m</i> -Diethylbenzene, <i>p</i> -Diethylbenzene, 1,2,3-Trimethylbenzene, 1,2,4-Trimethylbenzene, 1,3,5-Trimethylbenzene

laser wavelength can be tuned, in order to selectively excite OH electronically on a single OH absorption line, here the  $Q_1(3)$  line of the  $A^2\Sigma^+(v'=0) - X^2\Pi(v''=0)$  vibronic band at 308 nm. OH resonance fluorescence emitted between 307 nm and 311 nm is collected by an assembly of large-diameter fused-silica lenses and narrow-band optical filters and is detected with a highly sensitive channel photomultiplier tube which is mounted perpendicular to the gas beam and the laser axis. The fluorescence is measured by gated photon counting using a time delay ( $\approx 50$  ns) to discriminate

the longer-lived OH fluorescence (150 ns lifetime at 3.5 hPa) from the instantaneous laser stray light ( $\approx 20$  ns duration). The signals are further corrected for solar straylight, which enters the measurement cells through the nozzle orifice and is measured after each laser-pulse in a separate time gate with a delay of 25  $\mu$ s. Furthermore, the laser is tuned periodically on- and off-resonance to distinguish the OH fluorescence signal from non-resonant laser excited background signals (Hofzumahaus et al., 1996). Thus, the OH fluorescence is spectroscopically determined as the difference

**Table 3.** Mean values of atmospheric parameters measured from 06:00 to 10:00 CNST and 12:00 to 16:00 CNST at Backgarden during 5–25 July 2006, when measured data for OH and  $k_{\text{OH}}$  were simultaneously available.

Parameter	Mean value	
	06:00–10:00	12:00–16:00
O <sub>3</sub> (ppb)	18	62
NO (ppb)	8.8	0.14
NO <sub>2</sub> (ppb)	16.9	1.4
HONO (ppb)	1.5	0.21
CO (ppb)	1140	420
CH <sub>4</sub> (ppm) <sup>a</sup>	2.5	1.9
Ethane (ppb) <sup>b</sup>	1.5	1.5
Ethene (ppb) <sup>b</sup>	3	3
Isoprene (ppb)	1.0	1.8
HC3 (ppb) <sup>c</sup>	6.8	1.4
HC5 (ppb) <sup>c</sup>	5.3	0.6
HC8 (ppb) <sup>c</sup>	4.0	0.2
OLI (ppb) <sup>c</sup>	0.5	0.07
OLT (ppb) <sup>c</sup>	2.9	0.64
TOL (ppb) <sup>c</sup>	8.3	1.2
XYL (ppb) <sup>c</sup>	2.8	0.16
H <sub>2</sub> O (% abs)	3.3	3
$k_{\text{OH}}$ (s <sup>-1</sup> )	40.6	17.9
Photolysis frequencies (s <sup>-1</sup> )		
O <sub>3</sub> → O <sup>1</sup> D	$0.61 \times 10^{-5}$	$2.6 \times 10^{-5}$
NO <sub>2</sub> → NO + O	$2.9 \times 10^{-3}$	$6.6 \times 10^{-3}$
HONO → NO + OH	$5.3 \times 10^{-4}$	$1.2 \times 10^{-3}$
HCHO → H <sub>2</sub> + CO	$1.14 \times 10^{-5}$	$2.9 \times 10^{-5}$
HCHO → H + HCO	$0.86 \times 10^{-5}$	$2.5 \times 10^{-5}$
Temperature (°C)	29.5	33.6
Pressure (hPa)	1001	998

<sup>a</sup> Fourier transform spectrometer measurements (P. Xie, personal communication, 2010); <sup>b</sup> Fixed value, from gas chromatography measurements of canister samples; <sup>c</sup> See VOC assignment in Table 2

between on- and off-resonance measurements. The amount of detected OH fluorescence integrated over successive laser pulses can be converted into an ambient radical concentration, of which the required sensitivity is determined by calibration (see below).

The major technical differences between the present and previous instrument version is the integration of more compact, light-weight components for the laser system, the vacuum pumps and the gated photon-counting system and a more convenient distribution of the 308 nm laser radiation by optical fibres rather than by beam-steering mirrors. The laser system used in this work consists of an intracavity frequency-doubled tunable dye-laser (Tintura, New Laser Generation) which is pumped by a frequency-doubled Nd-YAG laser (Navigator-I, Spectra Physics). The dye laser uses an intracavity etalon for line narrowing and provides

a stable laser bandwidth (7 GHz at 308 nm). This stability is an advantage compared to the previously used laser system where the bandwidth was very sensitive to laser alignment with corresponding need for frequent recalibration of the HO<sub>x</sub> measurement. The present laser system provides up to 100 mW of UV (308 nm) pumped by a laser power of about 4 W (532 nm). The 308 nm power is distributed between the HO<sub>x</sub> detection cells, the LP-LIF instrument and the wavelength reference cell by means of beam splitters in a ratio of 60:32:8. Due to a technical problem of the frequency-doubling device of the Nd-YAG laser during the field campaign, the total UV power was reduced to 60 mW in the beginning, decreasing further to 10 mW towards the end of the campaign. The laser radiation was delivered by a 6 m long optical multimode fibre (QMMJ-55HP-UVVIS-200/240 μ, AMS Technologies) with an effective transmission of about 50–70 % to the detection cells. In- and outcoupling of the laser beam was achieved by AR-coated plano-convex quartz lenses ( $f = 25$  mm and 50 mm, respectively). For fluorescence detection, gated channel-photomultipliers (C1943P, Perkin Elmer) were connected to a gated photon-counter card (PMS300, Becker und Hickl GmbH) and gating signals were provided by a digital delay generator (DDG, Becker und Hickl GmbH) triggered by the laser system. The dry-vacuum pump (IPX500, BOC-Edwards) is connected to each detection chamber by separate flexible metal-bellow tubes (40 mm diameter) including motorized butterfly valves (MKS153), in order to stabilize the pressure in the cells to better than  $\pm 0.1$  mbar.

During the PRD campaign, the laser was tuned periodically to on- and off-resonance wavelength positions with integration times of 40 s and 8 s, respectively. Including some overhead time for laser scanning, a typical time resolution of 40–70 s was achieved for the HO<sub>x</sub> measurements. The instrument was calibrated with known amounts of OH and HO<sub>2</sub> radicals which were generated in a flow of synthetic air by photolysis of water vapor at 185 nm from a low-pressure discharge mercury lamp (for details, see Holland et al., 2003; Fuchs et al., 2011). The calibration source was recently tested in intercomparisons against absolute measurement techniques for OH (Schlosser et al., 2006, 2009), confirming the estimated accuracy ( $\pm 10$  %,  $1\sigma$ ) of the calibration method. At PRD, successive calibration measurements showed an unusually large  $1\sigma$  variability by 8.7 % and 13.6 % for OH and HO<sub>2</sub>, respectively, from day to day. This variability is about a factor of two larger than usual and suggests uncontrolled changes of the instrumental detection sensitivity. Since no trend was observed in the calibration data, an average calibration factor was applied for the campaign. The observed variability adds to the calibration uncertainty which is estimated to be 20 % ( $1\sigma$ ) in total. OH and HO<sub>2</sub> interferences caused by ambient O<sub>3</sub> were corrected by an amount of  $(6 \pm 2) \times 10^3$  cm<sup>-3</sup> and  $2 \times 10^4$  cm<sup>-3</sup>, respectively, per ppb of ozone. The correction was applied as only ozone dependent. A possible water-vapor dependence

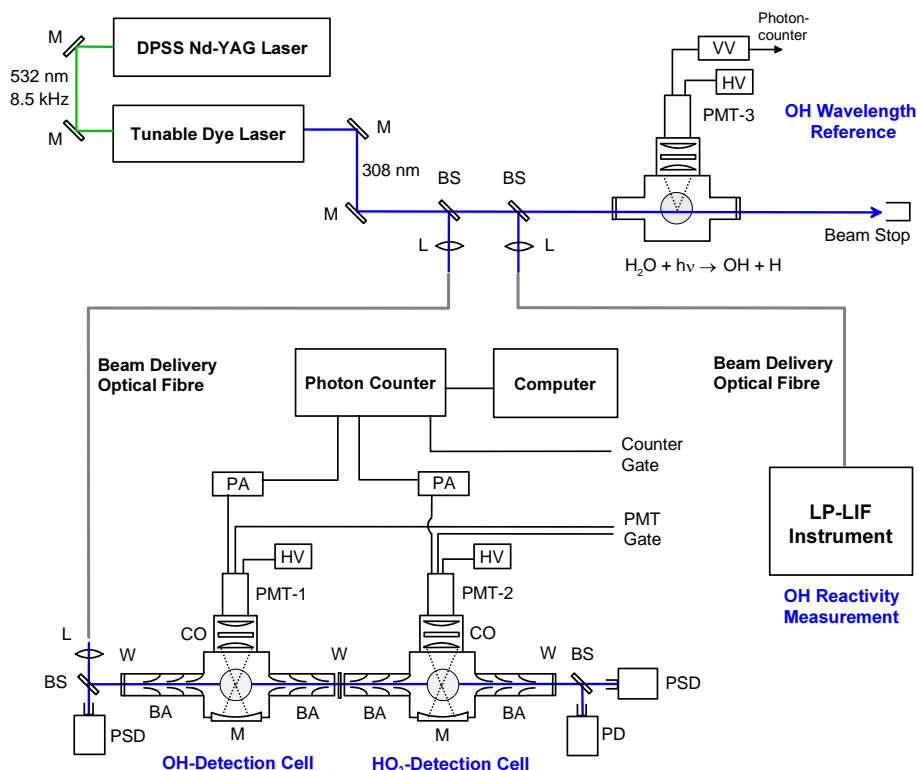


**Fig. 2.** Schematic drawing of the LIF system. Laser radiation (308 nm) from a tunable dye laser is distributed by beam steering optics (M, BS, L) and optical fibres to (a) a pair of independent detection chambers for measurement of OH and HO<sub>2</sub> concentrations, (b) a laser photolysis laser-induced fluorescence (LP-LIF) instrument for measurement of  $k_{\text{OH}}$ , and (c) a wavelength reference cell in which photolytically generated OH is monitored by LIF. Note that the sampled ambient air is flowing through the low-pressure detection chambers perpendicular to the optical plane shown in the figure. Abbrev.: M mirror, BS beam splitter, L lens, W quartz window, CO fluorescence collection optics, BA laser baffle arm, PD photodiode, PSD position-sensitive photodiode, PMT photomultiplier tube, HV high voltage supply, PA preamplifier.

of the interference is covered by the specified error ( $\pm 30\%$ ) of the correction. The calculated interference was generally small (within the limit of detection) and not important for the daytime HO<sub>x</sub> concentrations. The detection limit of the 5 min averaged OH data is  $5 \times 10^5 \text{ cm}^{-3}$  before 18 July 2006, afterwards due to a reduced laser power, this number increased to  $1 \times 10^6 \text{ cm}^{-3}$ ; the detection limit of the 5 min averaged HO<sub>2</sub> data is  $(1-2) \times 10^6 \text{ cm}^{-3}$  before 18 July 2006,  $(2-3) \times 10^6 \text{ cm}^{-3}$  afterwards.

### 2.3 HO<sub>2</sub> measurement interference by RO<sub>2</sub>

Recent laboratory studies show that our HO<sub>2</sub> detection system exhibits a significant sensitivity to specific RO<sub>2</sub> species, which are converted to OH by a sequence of NO dependent reactions (Nehr et al., 2011; Fuchs et al., 2011). In general, RO<sub>2</sub> reacts in the gas expansion with the injected NO as fast as HO<sub>2</sub> and forms RO (Reaction R5). In case of simple alkoxy radicals, RO reacts predominantly with O<sub>2</sub> and produces HO<sub>2</sub> (Reaction R6). Because of the short reaction time (few milliseconds) and the strongly reduced O<sub>2</sub> number density in the gas expansion, the RO to HO<sub>2</sub> conver-

sion is slow and the following production of detectable OH is marginal. Experimental tests have shown that the corresponding interference by C<sub>1</sub>–C<sub>4</sub> alkyl peroxy radicals is generally not larger than about 5% (Stevens et al., 1994; Kanaya et al., 2001; Tan et al., 2001; Creasey et al., 2002; Holland et al., 2003; Ren et al., 2004), consistent with the new results by Fuchs et al. (2011). However, in case of RO<sub>2</sub> from OH reactions with alkenes and aromatics, the RO radicals formed in Reaction (R5) undergo unimolecular reactions and extremely fast decomposition to HO<sub>2</sub>. In this case, the NO-dependent Reactions (R5) and (R7) control the effective rate of RO<sub>2</sub> → HO<sub>2</sub> → OH conversion. A significant amount of RO<sub>2</sub> is eventually detected as OH in the HO<sub>2</sub> detection cell, resulting in relative detection sensitivities ( $\alpha_{\text{RO}_2}$ ) for specific RO<sub>2</sub> compared to HO<sub>2</sub> of larger than 50% (Nehr et al., 2011; Fuchs et al., 2011).

Experimental  $\alpha_{\text{RO}_2}$  values for peroxy radicals from selected VOCs of the groups of alkanes, alkenes, aromatics and OVOCs are shown in Fig. 3 (red symbols). They apply to the instrumental configuration used at PRD (Fuchs et al., 2011). Relative detection sensitivities for methyl peroxy and ethyl peroxy radicals are small with 4% and 7%, respectively;

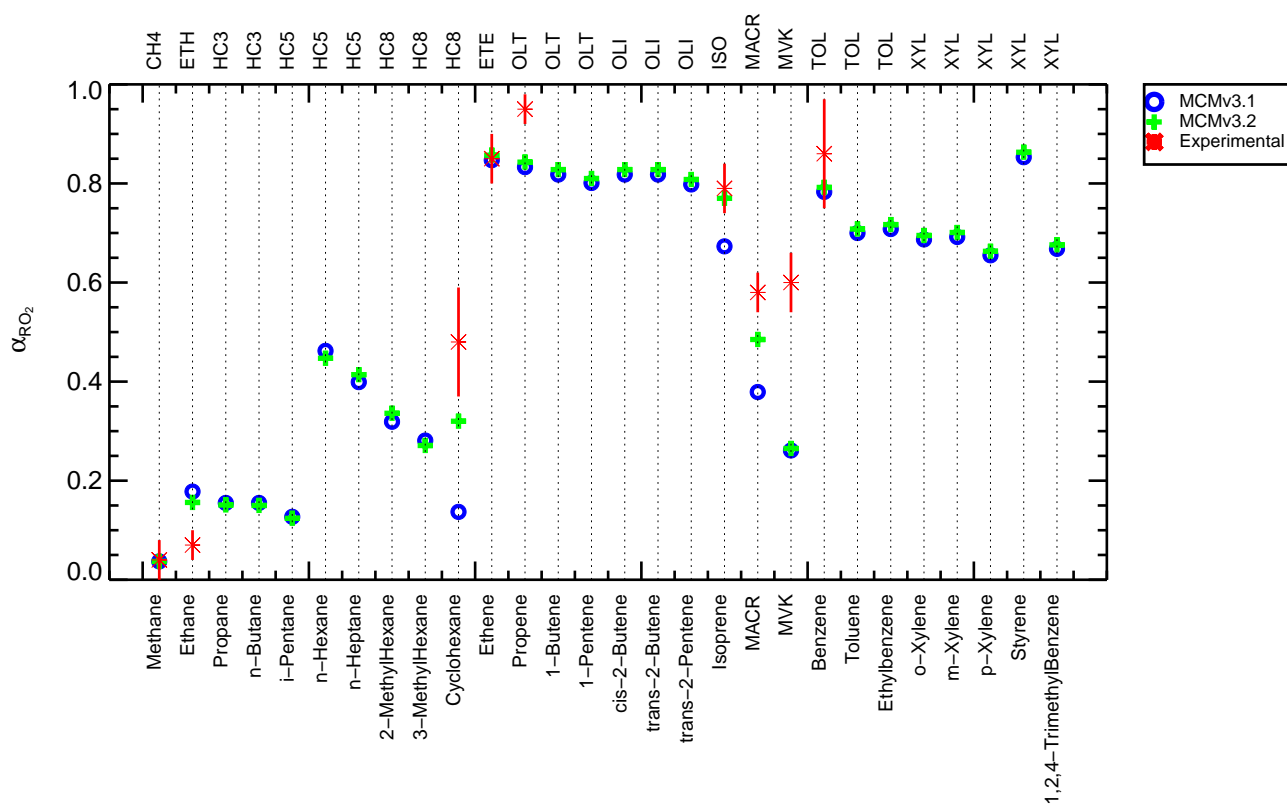


**Fig. 3.** Relative detection sensitivities ( $\alpha_{\text{RO}_2}^i$ ) for specific RO<sub>2</sub> compared to HO<sub>2</sub>. The experimental values (red stars) and their  $1\sigma$  error bars were determined for the instrument configuration applied at PRD for HO<sub>2</sub> detection (Fuchs et al., 2011). Modelled values (blue circles for MCMv3.1 and green crosses for MCMv3.2) are shown for major VOCs which contributed more than 90 % to the VOC reactivity in PRD. Original and mechanistic names of the VOCs are shown at the lower and upper x-axis, respectively.

but values are larger for peroxy radicals from cyclohexane (48 %), simple alkenes (85–95 %), isoprene (79 %), and benzene (86 %). Also the peroxy radicals from the OH reactions with major isoprene degradation products, methyl vinyl ketone (MVK) and methacrolein (MACR), have significant  $\alpha_{\text{RO}_2}$  values of about 60 %.

Model simulations of  $\alpha_{\text{RO}_2}$  are also presented in Fig. 3 covering the range of major VOCs which contributed more than 95 % to the VOC reactivity at PRD. The simulations are based on the Master Chemical Mechanism MCM v3.1 (blue symbols) by Saunders et al. (2003); Jenkin et al. (2003) and the more recent MCM v3.2 (green symbols; <http://mcm.leeds.ac.uk/MCM/>). Both reproduce the trend of the experimental values reasonably well, with improved agreement in the MCM v3.2 simulation for the peroxy radicals of isoprene, MACR and cyclohexane.

The HO<sub>2</sub> concentration measured by LIF, denoted as  $[\text{HO}_2^*]$ , is then expected to be the sum of the true HO<sub>2</sub> concentration and a systematic bias from the mixture of RO<sub>2</sub> species  $i$  which are detected with different relative sensitivities  $\alpha_{\text{RO}_2}^i$ .

$$[\text{HO}_2^*] = [\text{HO}_2] + \sum (\alpha_{\text{RO}_2}^i \times [\text{RO}_2]_i) \quad (1)$$

We have not attempted to correct the measured HO<sub>2</sub><sup>\*</sup> values in order to obtain true HO<sub>2</sub> concentrations, since RO<sub>2</sub> concentration measurements and their speciation were not available. However, a chemical box model is used to calculate concentrations for both HO<sub>2</sub> and HO<sub>2</sub><sup>\*</sup> (see below). The difference between these two concentrations can be considered an estimate of the effective instrumental interference from RO<sub>2</sub> at the conditions found at PRD.

## 2.4 The model

A zero-dimensional chemical box model was used to calculate concentrations of OH, HO<sub>2</sub>, HO<sub>2</sub><sup>\*</sup> and photochemical products of nitrogen and carbon compounds. In this work, we call the applied chemical mechanism RACM-MIM-GK (G = Geiger et al., 2003; K = Karl et al., 2006). It is based on the Regional Atmospheric Chemical Mechanism (RACM) (Stockwell et al., 1997) which was upgraded with the isoprene degradation scheme by Karl et al. (2006). The latter scheme is a modified version (26 reactions) of the mechanism by Geiger et al. (2003), who prepared a condensed version of the Mainz Isoprene Mechanism (MIM, 44 reactions)



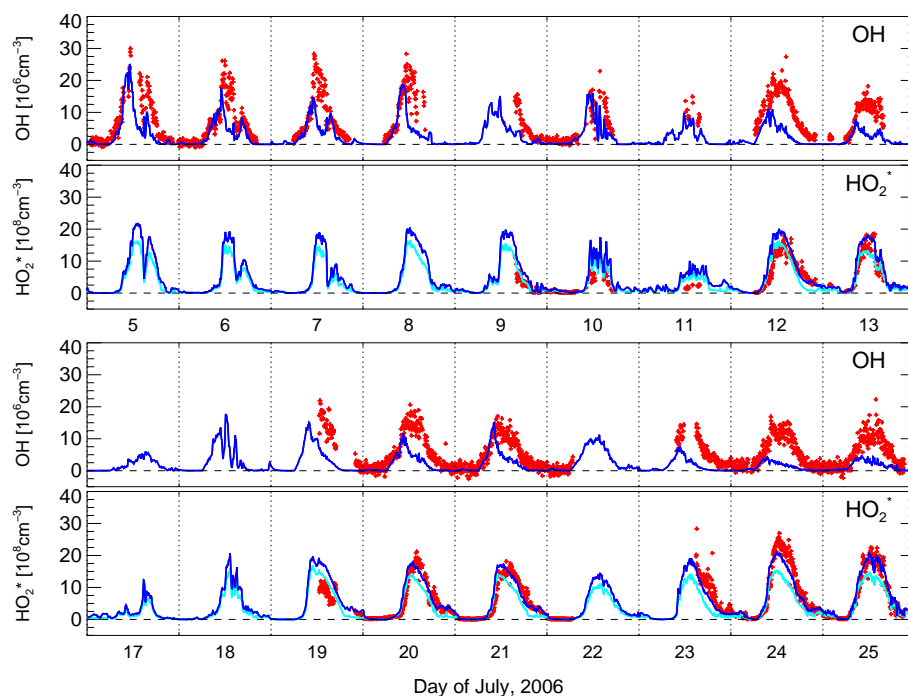


**Fig. 4.** Time series of 5 min-averaged measured and simulated (M0) concentrations of OH and HO<sub>2</sub><sup>\*</sup> at the Backgarden site during PRIDE-PRD2006 campaign. Experimental values are denoted by red symbols, modelled values by blue lines. Modelled values of HO<sub>2</sub> are represented by cyan lines. The difference between the lines for HO<sub>2</sub> and HO<sub>2</sub><sup>\*</sup> is the interference by RO<sub>2</sub> calculated by the base model (RACM-MIM-GK). Vertical dotted lines denote midnight.

(Pöschl et al., 2000). The complete mechanism of RACM-MIM-GK, which has been used before by Hofzumahaus et al. (2009) and Lou et al. (2010), is reported in Table S1 in the Supplement of this paper.

The model calculations were constrained to measurements of O<sub>3</sub>, HONO, NO, NO<sub>2</sub>, CO, CH<sub>4</sub>, C<sub>2</sub>–C<sub>12</sub> VOCs, photolysis frequencies, water vapor, ambient temperature and pressure. Table 2 explains the distribution of the measured VOC species into the lumped RACM-MIM-GK categories. Concentrations of ethane and ethene were set to fixed values of 1.5 ppb and 3 ppb, respectively, estimated from a few canister samples. The H<sub>2</sub> mixing ratio was assumed to be 550 ppb. The model was operated in a time-dependent mode with 5-min time resolution and 2 days spin-up time. An additional loss process with a lifetime of 24 h was assumed for calculated species, in order to represent dry deposition in the model. The lifetime corresponds to an assumed deposition velocity of 1.2 cm s<sup>-1</sup> and a well-mixed boundary layer height of about 1 km. Numerical sensitivity tests showed that the assumed deposition lifetime has a relatively small influence on the reactivity of the modelled oxidation products (e.g. OVOCs) (Lou et al., 2010). As a result, calculated OH and HO<sub>2</sub> concentrations vary by less than 5 % and 10 %, respectively, if the deposition rate is changed by a factor of two. Further sensitivity studies were performed to propagate the errors from the model boundary conditions and the reac-

tion rate constants of RACM-MIM-GK (Hofzumahaus et al., 2009) resulting in error estimates of about 40 % for the calculated OH, HO<sub>2</sub> and HO<sub>2</sub><sup>\*</sup> concentrations (for details, see Supplement).

For the calculation of HO<sub>2</sub><sup>\*</sup>, we used the  $\alpha_{\text{RO}_2}^i$  values which are listed for the major RACM peroxy radical species in Table 4. For RO<sub>2</sub> from OH reaction with CH<sub>4</sub> (methane), ETH (ethane), ETE (ethene), ISO (isoprene), MVK and MACR, the experimental data from Fig. 3 were used directly. For HC3, the experimental value of ETH was adopted, because the model predicted  $\alpha_{\text{RO}_2}^i$  values are almost equal for the respective peroxy radicals (Fig. 3). For HC5 and HC8,  $\alpha_{\text{RO}_2}^i$  was assumed to be the same as the experimental value for cyclohexane. For the peroxy radicals of OLI and OLT, the measured value for propene was used and for the aromatics TOL and XYL, the measured  $\alpha_{\text{RO}_2}^i$  for benzene was applied.

In the following, model runs with the RACM-MIM-GK are used as a reference which represents the framework of established photochemistry with classical, NO-dependent radical recycling. This base-case is denoted as M0. To explore possible reaction mechanisms which recycle OH radicals without NO, additional model runs were performed which incorporate assumed generic reaction pathways (M1–M2) or newly proposed mechanisms (M3–M6) into RACM-MIM-GK. Furthermore, the results from RACM-MIM-GK are compared to model runs based on the detailed MCM v3.1

**Table 4.** Relative RO<sub>2</sub> detection sensitivities ( $\alpha_{\text{RO}_2}$ ) used for the calculation of modelled HO<sub>2</sub><sup>\*</sup> concentrations.

RACM		$\alpha_{\text{RO}_2}$	Remark
Hydrocarbons <sup>a</sup>	Peroxy radicals <sup>b</sup>		
CH <sub>4</sub>	MO2	0.04 ± 0.04	exp. <sup>c</sup>
ETH	ETHP	0.07 ± 0.03	exp. <sup>c</sup>
HC3	HC3P	0.07 ± 0.03	estimated (ethane) <sup>d</sup>
HC5	HC5P	0.48 ± 0.18	estimated (cyclohexane) <sup>d</sup>
HC8	HC8P	0.48 ± 0.18	estimated (cyclohexane) <sup>d</sup>
ETE	ETEP	0.85 ± 0.05	exp. <sup>c</sup>
OLT	OLTP	0.95 ± 0.03	estimated (propene) <sup>d</sup>
OLI	OLIP	0.95 ± 0.03	estimated (propene) <sup>d</sup>
ISO	ISOP	0.79 ± 0.05	exp. <sup>c</sup>
MACR/MVK	MACP	0.59 ± 0.07	exp. <sup>c,e</sup>
TOL	TOLP	0.86 ± 0.13	estimated (benzene) <sup>d</sup>
XYL	XYLP	0.86 ± 0.13	estimated (benzene) <sup>d</sup>

<sup>a</sup> See Table 2; <sup>b</sup> Peroxy radicals formed from the OH+hydrocarbon reaction in 1 atm of air; <sup>c</sup> Experimental value and 1 $\sigma$  measurement error from Fig. 3; <sup>d</sup> Estimated; the experimental value for the hydrocarbon specified in paranthesis has been adopted. The 1 $\sigma$  error bar includes the experimental error of the specified hydrocarbon and the variability of the calculated  $\alpha_{\text{RO}_2}^i$  values in the corresponding RACM group, as shown in Fig. 3; <sup>e</sup> Mean value for MVK and MACR

(M7). An overview of the different model scenarios is given in Table 5 and the corresponding reaction mechanisms are listed in the Supplement of this paper. Details and results of the sensitivity runs are given in Sect. 4.3.

### 3 Results

#### 3.1 Observations of HO<sub>x</sub> and other photochemical parameters

During PRIDE-PRD2006, concentrations of OH and HO<sub>2</sub><sup>\*</sup> were measured from 5 to 25 July 2006. An overview of the 5 min-averaged data is shown in Fig. 4. Data gaps were caused by heavy rain during the typhoon BILIS (15–17 July 2006), by electric power failure (22 July 2006), and by instrument calibration or maintenance (i.e. 11 and 18 July 2006). The diurnal variations of the observed radicals followed a regular pattern from day to day, with maximum values around noon. To evaluate the variability of the daily peak values, mean values of the upper 0.05 percentiles of OH and HO<sub>2</sub><sup>\*</sup> were calculated for each day. Daily maximum OH concentrations varied from  $15 \times 10^6 \text{ cm}^{-3}$  to  $26 \times 10^6 \text{ cm}^{-3}$ , while daily maximum HO<sub>2</sub><sup>\*</sup> concentrations varied from  $3 \times 10^8$  to  $25 \times 10^8 \text{ cm}^{-3}$ . Significant HO<sub>x</sub> concentrations were measured during nighttime as well. While individual OH data points lie close to the limit of detection, hourly averaged nighttime values (at solar zenith angles larger than 90°) were in the range of  $0.2 \times 10^6 \text{ cm}^{-3}$  to  $5 \times 10^6 \text{ cm}^{-3}$  with an error of  $0.2 \times 10^6 \text{ cm}^{-3}$ . When averaged over the whole campaign, the mean nighttime value was  $2 \times 10^6 \text{ cm}^{-3}$ . For HO<sub>2</sub><sup>\*</sup> the hourly averaged nighttime val-

ues were in the range of  $0.1 \times 10^8 \text{ cm}^{-3}$  to  $10 \times 10^8 \text{ cm}^{-3}$  with an uncertainty of  $0.1 \times 10^8 \text{ cm}^{-3}$ . Over the whole campaign, the mean nighttime value of HO<sub>2</sub><sup>\*</sup> was  $2 \times 10^8 \text{ cm}^{-3}$ . The origin of nighttime HO<sub>x</sub> will be analyzed in a separate publication.

In order to characterize the encountered air masses from a photochemical point of view, time series of important parameters influencing the radical concentrations are presented in Fig. 5.  $j(\text{O}^1\text{D})$  and  $j(\text{NO}_2)$  showed regular diurnal patterns with high noontime values that reached up to  $4 \times 10^{-5} \text{ s}^{-1}$  and  $1 \times 10^{-2} \text{ s}^{-1}$ , respectively. Relatively small daytime values were observed on 15–17 July 2006 when the sky was covered by a dark cloud layer during typhoon BILIS. High concentrations of NO (often more than 10 ppb) were measured in the morning hours, while low concentrations below 1 ppb prevailed in the afternoon. Strong nighttime emissions from diesel engines were identified by enhanced values of light-absorbing carbon (LAC) measured at the PRD site by Garland et al. (2008). They found that the ratio of LAC to CO was highly variable throughout the campaign, indicating a complex mix of different combustion sources. Anthropogenic emissions from combustion activities might be the cause for the morning peak of NO, whereas a ban of large diesel-powered trucks during daytime, the enlarged boundary layer height and photochemical oxidation of NO<sub>x</sub> may be the reason for the low NO concentrations in the afternoon. The diurnal characteristic of NO<sub>2</sub> is similar to that of NO, but large concentrations of NO<sub>2</sub> often appear near midnight probably produced by titration of O<sub>3</sub> with freshly emitted NO. Ozone showed an anti-correlated diurnal variation compared to NO<sub>2</sub>. Peak values of O<sub>3</sub> mostly appear around noon or afternoon hours,

**Table 5.** Chemical mechanisms used in box model simulations of HO<sub>x</sub> for PRIDE-PRD2006.

Simulation	Chemical mechanisms*
M0	RACM-MIM-GK (base case) mechanism by Karl et al. (2006)
M1	as M0, with generic recycling reactions added as proposed by Hofzumahaus et al. (2009): RO <sub>2</sub> + X → HO <sub>2</sub> and HO <sub>2</sub> + X → OH
M2	as M0, with a single generic recycling reaction added: HO <sub>2</sub> + Y → OH
M3	as M0, with additional OH-forming channels in reactions of acyl peroxy + HO <sub>2</sub> and β-keto peroxy + HO <sub>2</sub> reactions
M4	as M3, with the OH-reforming mechanism by Paulot et al. (2009), in which reactions of OH with isoprene hydroxyhydroperoxides produce epoxides and prompt OH
M5	as M4, with the LIM0 scheme by Peeters and Müller (2010) incorporated, in which isoprene hydroxyperoxy radicals produce prompt HO <sub>2</sub> and HPALDs, followed by HPALDs photolysis. Two variants are tested: a: HPALDs + hν → OH + HO <sub>2</sub> + products b: HPALDs + hν → 3 OH + HO <sub>2</sub> + products
M6	as M3, with OH-formation from the reaction of isoprene hydroxyperoxy radicals with HO <sub>2</sub> as proposed by Lelieveld et al. (2008) and Butler et al. (2008). Two variants are tested: a: ISOP + HO <sub>2</sub> → 2OH + products b: ISOP + HO <sub>2</sub> → 4OH + products
M7	MCMv3.1(Saunders et al., 2003; Jenkin et al., 2003)

\* A detailed description and a listing of the mechanisms M0–M6 can be found in the Supplement of this paper.

indicating local photochemical ozone production (Lu et al., 2010). Relatively high concentrations of HONO were observed at the PRD site during early morning hours (about 1 ppb) and noon time (about 200 ppt). Details of the HONO budget are discussed by Li et al. (2011). CO concentrations had typical noontime values around 400 ppb. Spikes in the CO data set indicate scattered sources and inhomogeneities of the advected air mass. This is consistent with observed biomass burning activities close to the site and in the PRD region as a whole.

Since the site is located in a forested region, large isoprene concentrations can appear during daytime. As discussed by Lou et al. (2010), daily peak isoprene concentrations were correlated to the wind direction. For the prevailing southerly wind direction, the air had to travel over a large water reservoir and daily peak isoprene concentration were typically 1–2 ppb. For northerly wind directions (13–14 July and 23–25 July 2006), emissions from nearby plants or agriculture fields could directly influence the site and daily peak isoprene concentrations approached 5–6 ppb then. A biomass burning event on 23–25 July 2006 was identified by analysis of measured optical aerosol properties (Garland et al., 2008; Rose et al., 2010). Thus, the high isoprene concentration during this event could also have been caused by stress-induced plant emissions.

### 3.2 Base-case model results for HO<sub>x</sub>

Model calculated results (M0) for OH and HO<sub>2</sub><sup>\*</sup> are compared to the measured time series in Fig. 4. For OH, the base-case model shows diurnal patterns that are systematically different from the observations. During morning hours, modelled and measured concentrations always agree well, while in the afternoon the model underestimates the observed OH by a factor of 2 to 8. On the other hand, observations of HO<sub>2</sub><sup>\*</sup> are much better reproduced by the model. This picture using the full time resolution of observed data is consistent with what has been reported previously (Hofzumahaus et al., 2009) using diurnally averaged boundary conditions for modelling (see also Fig. S1 in the Supplement). It is interesting to note that the measured total OH reactivity, *k*<sub>OH</sub>, is reproduced well to within ±20 % by the model during daytime (Lou et al., 2010). The agreement exists in the morning and afternoon, and is independent of how well the model describes the OH concentration. Since the model simulates the total OH sinks (expressed by *k*<sub>OH</sub>) quite well, the large discrepancies between modelled and measured OH in the afternoon indicate missing OH production in the model.

The model has been used to simulate both ambient HO<sub>2</sub> and measured HO<sub>2</sub><sup>\*</sup>, which are shown in Fig. 4 for comparison. The difference between the two quantities can be

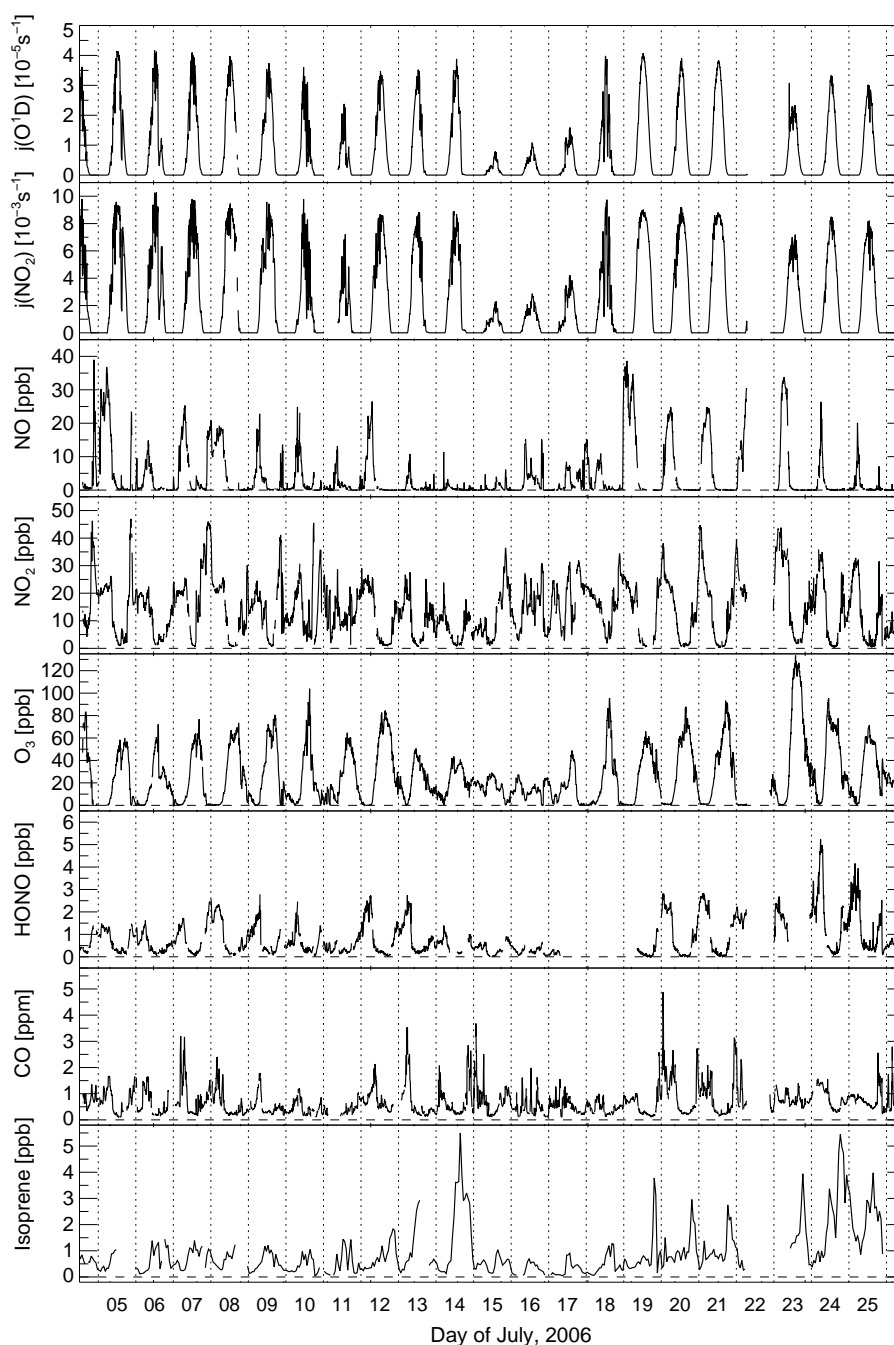


**Fig. 5.** Time-series of measured  $j(\text{O}^1\text{D})$ ,  $j(\text{NO}_2)$ , NO,  $\text{NO}_2$ ,  $\text{O}_3$ , HONO, CO and isoprene at PRD Backgarden from 5 July to 25 July 2006. Vertical lines denote midnight.

considered a model estimate of the HO<sub>2</sub> interference from ambient RO<sub>2</sub>. It is quite small during morning hours, while it becomes larger in the afternoon going along with notable day to day variability. On average, the model estimated interference is about 30 % at daytime. It should be noted that this estimate is model dependent and has a large uncertainty since the model cannot reproduce the observed OH correctly (see Sect. 4.3).

The radical budget of HO<sub>x</sub> and the related RO<sub>x</sub> is analyzed in Figs. 6 and 7 using chemical turnover rates determined by the base model (M0). Figure 6 shows the mean diurnal profiles of the production and loss rates of RO<sub>x</sub>. During daytime, the primary OH production,  $P(\text{OH})$ , and primary HO<sub>2</sub> production,  $P(\text{HO}_2)$ , were the dominant part of  $P(\text{RO}_x)$ . O<sub>3</sub> and HONO photolysis reactions constituted the major part of  $P(\text{OH})$ , while HCHO photolysis (about

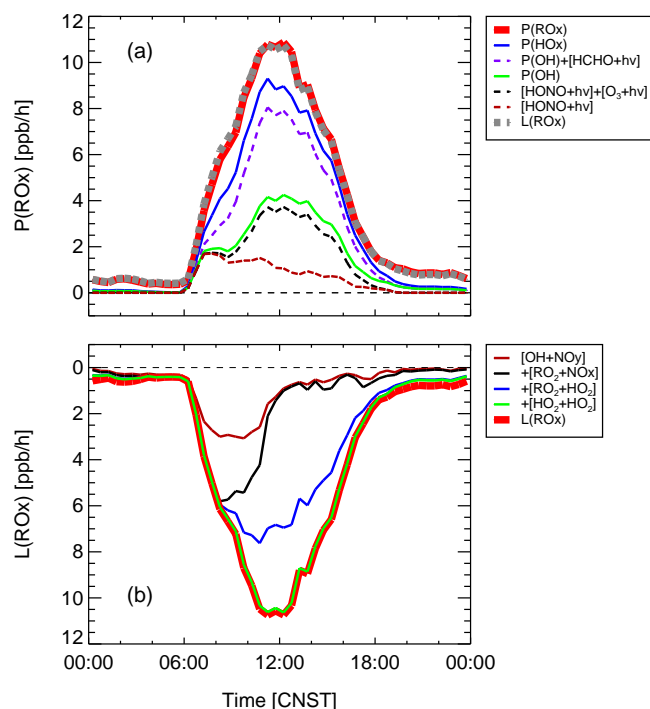


**Fig. 6.** Production (a) and loss rates (b) of RO<sub>x</sub> radicals (= OH + HO<sub>2</sub> + RO<sub>2</sub>) calculated with RACM-MIM-GK (M0). Panel (a): breakdown of the primary RO<sub>x</sub> production resulting from photolytic processes and ozonolysis.  $P(\text{OH})$ ,  $P(\text{HO}_x)$ , and  $P(\text{RO}_x)$  denote total, primary production rates of OH, HO<sub>x</sub>, and RO<sub>x</sub>, respectively. Panel (b): breakdown of the RO<sub>x</sub> loss caused by radical termination reactions. The brown solid line denotes the loss rate by OH + NO<sub>y</sub>, the black solid line by OH + NO<sub>y</sub> and RO<sub>2</sub> + NO<sub>x</sub>, etc. The total RO<sub>x</sub> loss rate is given by  $L(\text{RO}_x)$  which is equal in magnitude to  $P(\text{RO}_x)$  shown in panel (a). Legends: the expressions embedded in square brackets represent the corresponding chemical conversion rates.

3–4 ppb h<sup>-1</sup> during noon time) dominated  $P(\text{HO}_2)$ . The next important processes were the photolysis of dicarbonyls including glyoxal (GLY),  $\alpha$ -carbonyl aldehydes (MGLY) and unsaturated dicarbonyls (DCB). In the early morning, HONO photolysis was the most important primary source of HO<sub>x</sub>, which contributed 60–70 % of  $P(\text{HO}_x)$  between 07:00 and 08:00 CNST. A recently proposed new primary OH source, the reaction of excited NO<sub>2</sub> with H<sub>2</sub>O (Li et al., 2008), has been examined as well. The photolysis frequency for the production of excited NO<sub>2</sub> was calculated from measured actinic flux spectra, assuming that excited NO<sub>2</sub> is formed beyond the photodissociation threshold (420 nm) up to wavelength of 700 nm with unity quantum yield. The estimated radical production rate from this channel was only about 0.1 ppb h<sup>-1</sup> at 08:30 CNST (SZA = 60°) which is almost negligible at our conditions. As indicated by the overlapping grey dashed and red solid lines in Fig. 6a, the total RO<sub>x</sub> production is balanced by equally large RO<sub>x</sub> sinks,  $L(\text{RO}_x)$ , in the model. As shown

by Fig. 6b,  $L(\text{RO}_x)$  is dominated in the morning by OH reactions with odd nitrogen compounds and RO<sub>2</sub> reactions with NO<sub>x</sub> yielding nitrates and PANs. In the afternoon, self reactions of HO<sub>2</sub> or RO<sub>2</sub> and cross reactions between HO<sub>2</sub> and RO<sub>2</sub> are dominant.

In Fig. 7a, b, the rates of OH reactions yielding HO<sub>2</sub> and RO<sub>2</sub> are specified. As discussed for the correspondingly measured  $k_{\text{OH}}$  (Lou et al., 2010), half of the OH loss can be explained by the measured trace gases given in Table 1 and half by modelled daughter products of isoprene, alkenes and aromatics. OH → HO<sub>2</sub> conversion is mainly caused by reaction of OH with CO and formaldehyde throughout the day. During early morning hours, the total OH → RO<sub>2</sub> conversion rate is dominated by oxidation reactions of alkenes (propene, butenes, pentenes) and aromatics (styrene, toluene, xylenes, trimethylbenzenes), while it is dominated by isoprene and its degradation products in the afternoon. This is reflected in the RO<sub>2</sub> speciation within different NO<sub>x</sub> regimes (see Fig. S2 and Table S8, Supplement).

Recycling rates for RO<sub>2</sub> → HO<sub>2</sub> and HO<sub>2</sub> → OH are specified in Fig. 7c, d, respectively. RO<sub>2</sub> → HO<sub>2</sub> conversion is dominated by NO reactions with MO<sub>2</sub>, ISOP and MACP. Here, MO<sub>2</sub> is predominantly formed from oxidation of methane, isoprene and alkenes. Figure 7d shows that HO<sub>2</sub> → OH recycling (red line) is mainly caused by the reaction HO<sub>2</sub> + NO (blue line). It is nearly balanced by HO<sub>2</sub> formation through OH → HO<sub>2</sub> plus RO<sub>2</sub> → HO<sub>2</sub> reactions (dark red line), demonstrating that the HO<sub>2</sub> budget is mainly controlled by cycling reactions rather than by primary production and termination reactions. Furthermore, it can be noted that the total peroxy radical formation rate, i.e. the sum of  $R(\text{OH} \rightarrow \text{HO}_2)$  and  $R(\text{OH} \rightarrow \text{RO}_2)$  (violet dashed line) agrees most of the day with the recycling rate HO<sub>2</sub> → OH. A relative large difference is found only in the afternoon, indicating inefficient recycling to OH in the RO<sub>x</sub> propagation implemented in the base model, consistent with the analysis of  $L(\text{RO}_x)$  in Fig. 6b.

## 4 Discussion

HO<sub>x</sub> concentrations observed during PRIDE-PRD2006 are the highest so far reported for urban and suburban environments at summer time (Table 6). In Mexico City (located at a similar latitude and also in a developing country) relative small HO<sub>x</sub> concentrations were observed. Among the other cities, which are located in developed countries like US, Europe and Japan, measurements at Nashville and New York City showed relative high HO<sub>x</sub> concentrations that approach the levels of PRD. One reason for the high radical concentrations at PRD is the strong subtropical insolation leading to large radical production rates by photolysis (cf. Fig. 6a). In fact, the mean noontime  $j(\text{O}^1\text{D})$  value was larger during PRIDE-PRD2006 than during other campaigns listed in Table 6. The meteorological conditions and high precursor

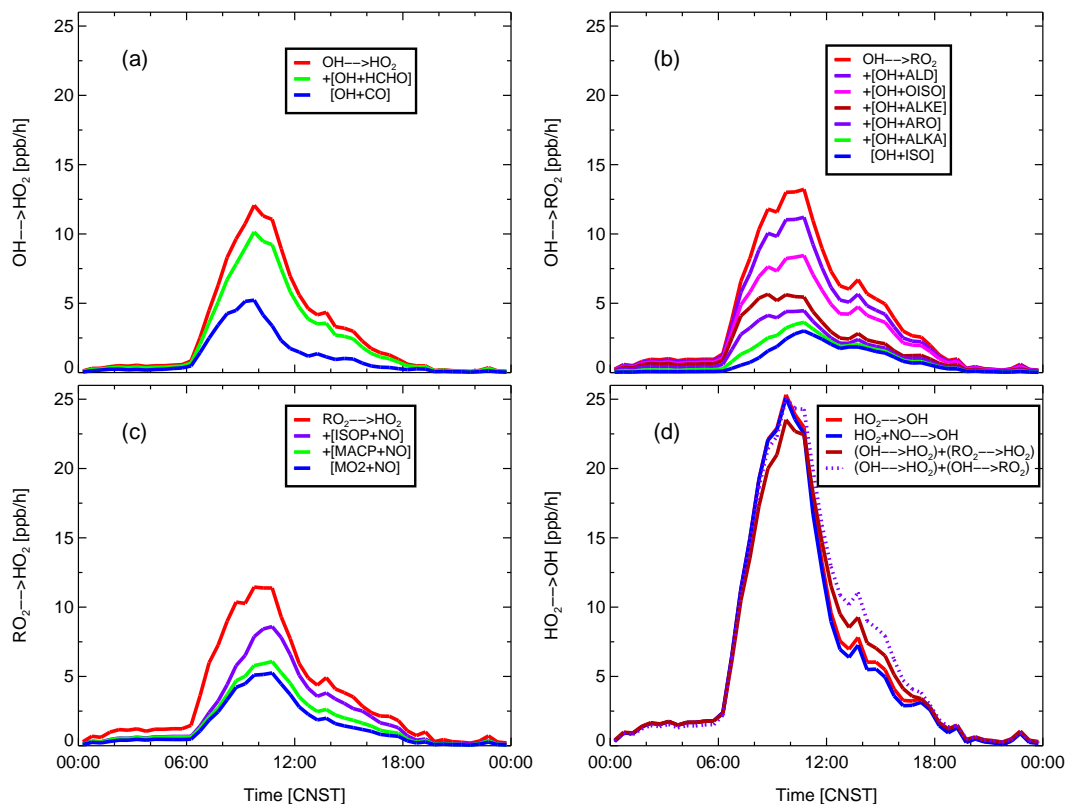


**Fig. 7.** Radical conversion rates (red—) of (a)  $\text{OH} \rightarrow \text{HO}_2$ , (b)  $\text{OH} \rightarrow \text{RO}_2$ , (c)  $\text{RO}_2 \rightarrow \text{HO}_2$ , and (d)  $\text{HO}_2 \rightarrow \text{OH}$ , calculated with RACM-MIM-GK (M0). The cumulative contributions of dominating reactions are presented as explained in Fig. 6. Panel (d): total OH loss and total  $\text{HO}_2$  production, both confined to radical conversion reactions, are displayed by the dotted violet and solid brown lines, respectively.

concentrations (e.g.  $\text{O}_3$ , water vapor, HONO) favored large  $\text{HO}_x$  radical concentrations. Taking into account the high mean OH reactivity of  $20 \text{ s}^{-1}$  observed at Guangzhou during daytime, the large measured OH concentrations indicate exceptional intense photochemistry in Southern China. The significant model underprediction of OH in the afternoon (Fig. 4) implies that the known OH sources alone cannot explain the high OH daytime values. In order to characterize the missing chemical processes that sustain the high experimental OH values, the discrepancies between modelled and measured OH will be investigated in the following discussion as a function of other atmospheric parameters.

When comparing the reported  $\text{HO}_2$  values in Table 6, it must be kept in mind that the data from different campaigns were measured by similar LIF techniques, which all rely on chemical  $\text{HO}_2$  conversion. It is likely that the interference from specific  $\text{RO}_2$  species, described in Sect. 2.3, has influenced all LIF measurements of  $\text{HO}_2$  compiled in Table 6. Since the abundance and speciation of  $\text{RO}_2$  is certainly different for the various campaigns, a relatively large, not well quantified uncertainty has to be attached to the  $\text{HO}_2$  comparison among different locations.

#### 4.1 $j(\text{O}^1\text{D})$ and $\text{NO}_x$ dependence of OH

A high correlation between OH and  $j(\text{O}^1\text{D})$  was observed over the whole range of atmospheric conditions during the PRD campaign, with a linear correlation coefficient of  $r^2 = 0.81$  (Fig. 8a). In past campaigns, similar high correlations were observed (Rohrer and Berresheim, 2006, and reference therein), but at conditions with much lower VOC reactivities. For limiting cases with low or high  $\text{NO}_x$  concentrations, theoretical explanations were attempted using reaction schemes with a simplified VOC chemistry (e.g. Poppe et al., 1995). But even for the limiting cases in the steady state calculation of OH, the role of other photolysis processes (e.g. of HCHO and  $\text{NO}_2$ ) is clearly visible and should in principle disturb the linear correlation between OH and  $j(\text{O}^1\text{D})$ . Ehhalt and Rohrer (2000) performed a detailed analysis of this relationship based on observational results derived during the POP-CORN campaign in rural Germany. They showed that the observed correlation of OH and  $j(\text{O}^1\text{D})$  is just fortuitously linear, resulting from the combined influence of all photolytic processes on OH, which are highly correlated among themselves. According to this analysis, a power-law function with an exponential parameter close to unity is more suitable. Based on the analysis of a five year OH dataset,

**Table 6.** Noontime maxima of measured HO<sub>x</sub> concentrations at urban and suburban sites during summer time. All the cited radical measurements were performed by LIF techniques.

Site	Month, year	OH <sup>a</sup> (10 <sup>6</sup> cm <sup>-3</sup> )	HO <sub>2</sub> <sup>a,b</sup> (10 <sup>8</sup> cm <sup>-3</sup> )	<i>j</i> (O <sup>1</sup> D) <sup>c</sup> (10 <sup>-5</sup> s <sup>-1</sup> )	Reference
Los Angeles (34° N)	Sep 1993	5–7	1.4–2	–	George et al. (1999)
Berlin (52.9° N)	Jul–Aug 1998	4–8	2–8	1.5	Holland et al. (2003)
Birmingham (52.4° N)	Jun 1999	2–9	1.5–10	1.5 <sup>d</sup>	Emmerson et al. (2005)
Nashville (36.2° N)	Jun–Jul 1999	7.5–20	2.5–20	3 <sup>e</sup>	Martinez et al. (2003)
New York City <sup>f</sup> (40.7° N)	Jun–Aug 2001	3–33	0.8–10	2.5	Ren et al. (2003)
Mexico City <sup>f,g</sup> (19.4° N)	Apr 2003	8–13	5–20	3.4 <sup>h</sup>	Shirley et al. (2006)
London (51.7° N)	Jul–Aug 2003	1–6	<0.5–2	1–2 <sup>a</sup>	Emmerson et al. (2007)
Tokyo (35.6° N)	Jul–Aug 2004	5–13	0.7–14	2.5	Kanaya et al. (2007b)
Houston (29.7° N)	Aug 2000	≈18	≈7	3.0	Mao et al. (2010)
Houston (29.7° N)	Sep 2006	≈14	≈10	3.0	Mao et al. (2010)
Guangzhou (23.5° N)	Jul 2006	15–26	3–25	3.5	This work

<sup>a</sup> Range of reported daily noontime maxima; <sup>b</sup> Observed HO<sub>2</sub> values by LIF instruments uncorrected for RO<sub>2</sub> interferences (see Sect. 2.3); <sup>c</sup> Mean noontime value; <sup>d</sup> Value from a single day (Harrison et al., 2006); <sup>e</sup> Value from a single day (Thornton et al., 2002); <sup>f</sup> The radical concentrations in this table is 1.64 times larger than that reported originally according to Mao et al. (2010).; <sup>g</sup> Located at about 2240 m above sea level; <sup>h</sup> Scaled to be 1.36 higher than in New York City during summer 2001 (Ren et al., 2003) as stated in Shirley et al. (2006)

a simple empirical model was constructed to describe this relation (Rohrer and Berresheim, 2006):

$$[\text{OH}] = a \times (j(\text{O}^1\text{D})/10^{-5} \text{ s}^{-1})^b + c \quad (2)$$

The pre-exponential coefficient, *a*, incorporates the condensed information of the chemical conditions (e.g. NO<sub>x</sub> or VOCs) at a certain location. Exponent *b* reflects the combined effects of all photolytic processes (i.e. *j*(O<sup>1</sup>D), *j*(NO<sub>2</sub>), *j*(HONO), *j*(HCHO)). These photolytic processes either play a role in primary production processes of HO<sub>x</sub> radicals or influence its recycling processes. Finally, the offset parameter *c* accounts for non-photolytic OH sources. When applied to the scatter plot in Fig. 8a, a Levenberg-Marquard fit yields *a* = 5.6 × 10<sup>6</sup> cm<sup>-3</sup>, *b* = 0.68 and *c* = 2.3 × 10<sup>6</sup> cm<sup>-3</sup>, providing a parameterized description for the PRD conditions.

For comparison to other campaigns, a linear fit is more appropriate, since often only linear coefficients are published. The disadvantage in using linear coefficients is a short-fall in the description of twilight conditions for OH. The slope of a linear fit to the PRIDE-PRD2006 observations is 4.0 × 10<sup>11</sup> s cm<sup>-3</sup> and the offset 2.4 × 10<sup>6</sup> cm<sup>-3</sup>. In the marine boundary layer, reported slopes are relatively low, ≤ 2 × 10<sup>11</sup> s cm<sup>-3</sup> (Berresheim et al., 2003; Brauers et al., 2001; Smith et al., 2006), while in continental regions reported values lie in the range of (2–4) × 10<sup>11</sup> s cm<sup>-3</sup> (Holland et al., 2003; Rohrer and Berresheim, 2006; Ehhalt and Rohrer, 2000). The slope for PRIDE-PRD2006 is at the upper limit of previous continental field observations, which again indicates an intense photochemical activity in the PRD region.

The model simulation (M0) cannot reproduce the high correlation between measured OH and *j*(O<sup>1</sup>D). Unlike the ex-

perimental scatter plot (Fig. 8a), the plot of calculated OH versus measured *j*(O<sup>1</sup>D) is split into two groups of data forming a “V”-like shape (Fig. 8b). The upper branch corresponds to morning hours, when modelled and observed OH are in good agreement (cf. Fig. 4). The lower branch of the “V” represents afternoon data, when the model severely underpredicts OH. One major difference between the two branches is the level of NO<sub>x</sub>, which was high in the morning and low in the afternoon (Table 3). Interestingly, the empirical relationship between measured OH and *j*(O<sup>1</sup>D) is not only compact in both NO<sub>x</sub> regimes, but both subsets of data also overlap completely (Fig. 8a). Apparently, some unknown chemical mechanism which is missing in the base model stabilizes the ambient OH concentration. A similar tendency was noticed for a measured five-year OH record at Hohenpeissenberg, where the observed correlation between OH and *j*(O<sup>1</sup>D) was more stable and compact than could be explained by a chemical box model (Rohrer and Berresheim, 2006).

For inspection of the OH dependence on NO<sub>x</sub>, we remove the strong influence of *j*(O<sup>1</sup>D) by normalization as shown in Eq. (3).

$$[\text{OH}_{\text{Jnorm}}] = \frac{[\text{OH}]}{j(\text{O}^1\text{D})} \times \overline{j(\text{O}^1\text{D})} \quad (3)$$

Here,  $\overline{j(\text{O}^1\text{D})}$  denotes the mean value of the *j*(O<sup>1</sup>D) data set. To avoid using conditions during twilight for reasons discussed above, the data in this normalization analysis are restricted to *j*(O<sup>1</sup>D) larger than 1 × 10<sup>-5</sup> s<sup>-1</sup>. The NO<sub>x</sub> dependency of observed and model calculated OH<sub>Jnorm</sub> are denoted as small dots in Fig. 8c, respectively. In addition, trend lines are shown that were obtained by averaging OH<sub>Jnorm</sub> concentrations over equal ln([NO<sub>x</sub>]/ppb) intervals of 0.5.

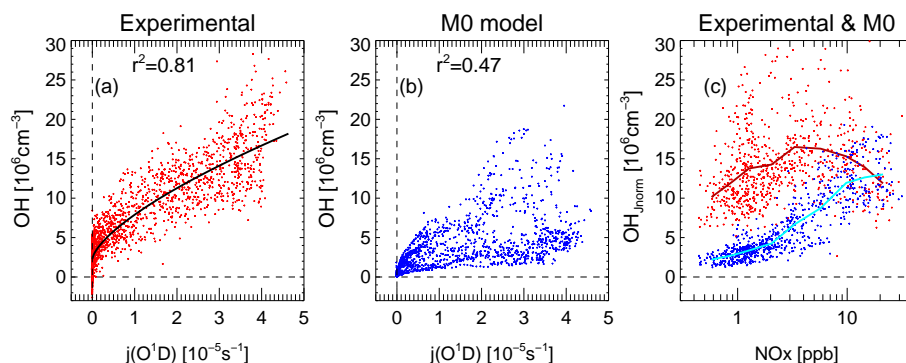


**Fig. 8.** Correlation of OH with  $j(\text{O}^1\text{D})$  and  $\text{NO}_x$  at PRD background. Panels (a, b) show the measured and modelled (M0) dependencies of OH on  $j(\text{O}^1\text{D})$ . The black line in panel (a) represents a Levenberg-Marquard fit to Eq. (2). The measured and modelled dependencies on  $\text{NO}_x$  are shown in panel (c) denoted by red and blue symbols, respectively. Here, the OH data were first selected by  $j(\text{O}^1\text{D}) > 1 \times 10^{-5} \text{ s}^{-1}$  and then normalized to  $j(\text{O}^1\text{D})$  (see text), denoted as  $\text{OH}_{\text{Jnorm}}$ . The solid lines give the averaged values of the measured (red) and modelled (blue)  $\text{OH}_{\text{Jnorm}}$  over equally spaced  $\ln([\text{NO}_x]/\text{ppb})$  intervals. Modelled curves for the scenarios M1, M2, M5b, M6b can be found in Fig. S3.

The mean measured  $\text{OH}_{\text{Jnorm}}$  is almost constant over the displayed  $\text{NO}_x$  range, showing a broad curvature with a relative maximum of about  $15 \times 10^6 \text{ cm}^{-3}$  at 3–4 ppb  $\text{NO}_x$  (Fig. 8c). In contrast, the model simulation predicts a steady increase of OH from low values at less than 1 ppb  $\text{NO}_x$  to a maximum OH concentration at 10–20 ppb  $\text{NO}_x$ . At the high end of observed  $\text{NO}_x$  values the set of modelled OH data points overlaps with the measured data, while the averaged data (solid lines) suggest different trends of modelled and measured OH towards higher  $\text{NO}_x$ . If we extrapolate the model curve for increasing  $\text{NO}_x$  at otherwise fixed conditions, we find that OH has a maximum concentration between 10 to 20 ppb  $\text{NO}_x$  and decreases thereafter (not shown). Since we have no corresponding OH observations, it remains open how well OH can be modelled at PRD at very high  $\text{NO}_x$ . The theoretically predicted  $\text{NO}_x$  dependence of OH is a result of two counteracting processes (Ehhalt, 1999; McKeen et al., 1997; Poppe et al., 1993; Weinstock et al., 1980). At low  $\text{NO}_x$ , OH increases with NO due to the recycling by  $\text{HO}_2 + \text{NO}$ , whereas at high  $\text{NO}_x$ , OH decreases as a result of the OH reaction with  $\text{NO}_2$ . This theoretical behaviour was confirmed for relatively clean rural air at POPCORN, where a nonlinear dependence with a maximum at 1 ppb  $\text{NO}_2$  was found in good agreement for measured and modelled OH (Ehhalt, 1999). The different behaviour of modelled and measured OH at PRD indicates that besides  $\text{NO}_x$  and  $j(\text{O}^1\text{D})$  other, yet unknown parameters may also strongly influence OH.

#### 4.2 NO and isoprene dependence of the measured-to-modelled OH ratio

To gain further insight into the shortcomings of the base model calculation M0, the ratio of measured-to-modelled OH,  $\text{OH}_{\text{obs}}/\text{OH}_{\text{mod}}$ , has been inspected as a function of NO, CO, VOCs and  $k_{\text{OH}}$ . A notable trend is found only for

NO and isoprene (Fig. 9a, b), with correlation coefficients  $r = -0.77$  and  $r = 0.48$ , respectively. Figure 9a displays a strong NO dependence of  $\text{OH}_{\text{obs}}/\text{OH}_{\text{mod}}$  with a smooth transition from ratios of about 8 at 0.02 ppb NO to unity ratio at NO mixing ratios larger than 1 ppb. This indicates that chemical processes are missing in the model which compete with NO dependent reactions and become dominant at low NO.

With respect to isoprene, two data clouds around 1 ppb and 3 ppb of isoprene are visible in Fig. 9b. For the combined data set, a weak positive correlation between  $\text{OH}_{\text{obs}}/\text{OH}_{\text{mod}}$  and isoprene seems to exist. No correlation is found for other investigated parameters. For example, indicators of anthropogenic activities like CO (especially from biomass burning) or benzene clearly show no correlation with  $\text{OH}_{\text{obs}}/\text{OH}_{\text{mod}}$  (Fig. 9c, d). Neither did we find a dependence on the total OH reactivity, nor a correlation with the VOC reactivity (not shown).

Figure 10a offers a more detailed inspection of the relationship between  $\text{OH}_{\text{obs}}/\text{OH}_{\text{mod}}$  and isoprene by color coding the data according to the concurrently measured NO mixing ratios. It can be seen that part of the trend of  $\text{OH}_{\text{obs}}/\text{OH}_{\text{mod}}$  vs. isoprene can be attributed to an anticorrelation between NO and isoprene. Isoprene was generally lower in the morning when NO was high and reached highest values in the afternoon when the NO mixing ratio was small. When the data in Fig. 10a are selected for low NO ( $< 0.5$  ppb), no significant trend with isoprene is found (red circles). Thus, the weak positive correlation in the whole data set between  $\text{OH}_{\text{obs}}/\text{OH}_{\text{mod}}$  and isoprene seems to be a consequence of the different  $\text{NO}_x$  levels of the two data clouds around 1 ppb and 3 ppb of isoprene. Given the small dynamic range of isoprene and the influence of NO, a functional dependence on isoprene cannot be postulated on the basis of our PRD data.



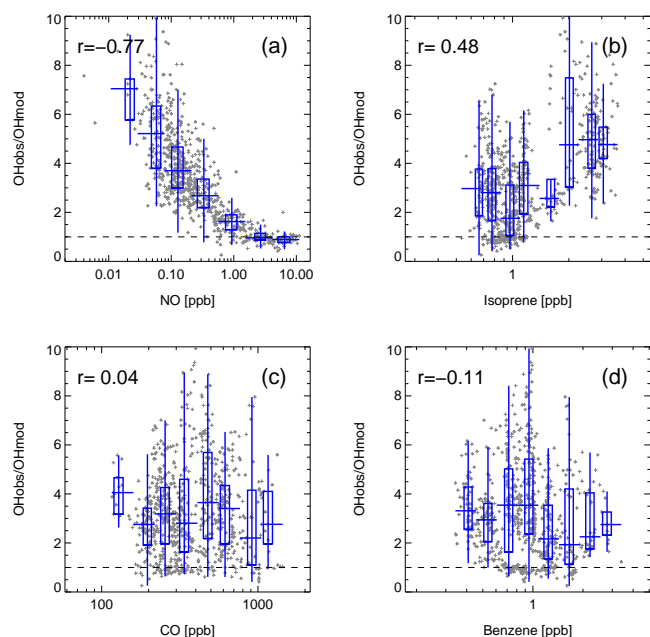


**Fig. 9.** Measured-to-modelled OH ratios,  $\text{OH}_{\text{obs}}/\text{OH}_{\text{mod}}$ , plotted versus the mixing ratios of (a) NO, (b) isoprene, (c) CO, and (d) benzene. The data have been filtered for  $j(\text{O}^1\text{D}) \geq 1 \times 10^{-5} \text{ s}^{-1}$  and are presented as individual data points (crosses) and in box-and-whisker style (the bottom and top of the boxes mark the lower and upper quartiles, respectively), horizontal lines denote median values, and the lower and upper whiskers the minimum and maximum values, respectively. Correlation coefficients,  $r$ , between  $\text{OH}_{\text{obs}}/\text{OH}_{\text{mod}}$  and the logarithmic values of NO, isoprene, CO and benzene are shown in corresponding panels as well.

A model underprediction of measured OH concentrations by up to an order of magnitude has been reported for forested areas, which are characterized by isoprene emissions and low NO<sub>x</sub> (Tan et al., 2001; Ren et al., 2008; Lelieveld et al., 2008; Pugh et al., 2010; Whalley et al., 2011). Figure 10b compares our  $\text{OH}_{\text{obs}}/\text{OH}_{\text{mod}}$  ratios with the results from these other studies. For this purpose, we use the PRD data selected for low NO (< 0.5 ppb) from Fig. 10a (red circles). The magnitude of the measured-to-modelled OH ratios of our study agree well with those from previous investigations, i.e. above deciduous forest in North-America during PROPHET (Tan et al., 2001) and INTEX-A (Ren et al., 2008), above the Amazonian rainforest during GABRIEL (Kubistin et al., 2010) and the Borneo rainforest during OP3 (Whalley et al., 2011). When all data sets are combined, a consistent trend of an OH model underprediction with increasing isoprene seems to emerge, as pointed out previously by Ren et al. (2008) and Kubistin et al. (2010).

While the experimental OH data from the different campaigns were measured by similar LIF techniques, differences exist in the chemical models that were applied for the OH simulations. Four different chemical mechanisms were used: RACM-MIM-GK for our study, RACM supplemented with

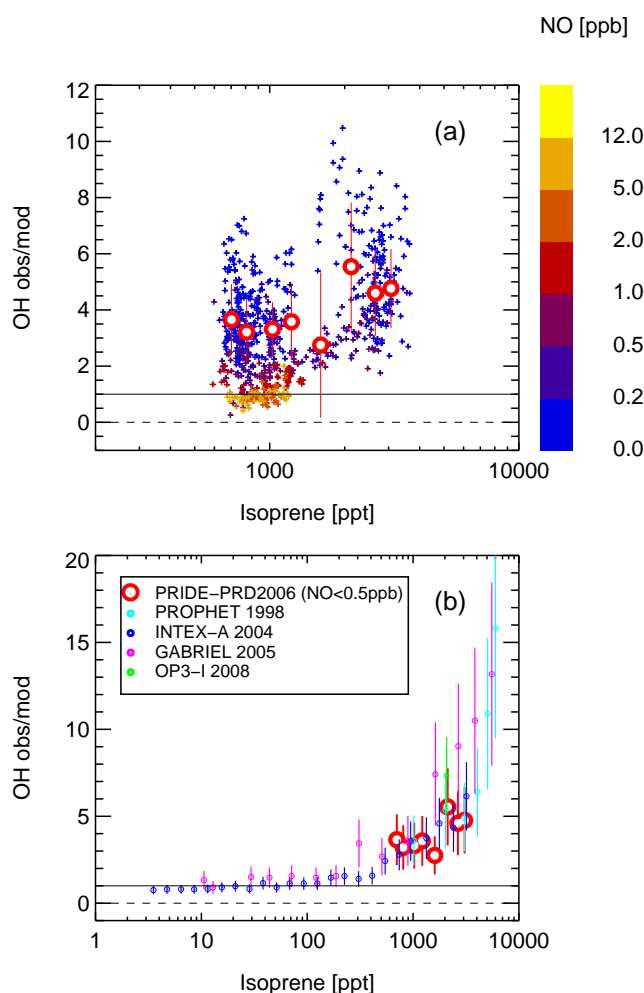


**Fig. 10.** The observed-to-modelled OH ratio as a function of isoprene at PRD background (a) and its comparison to ratios reported from other field campaigns (b). Panel (a): the individual data points from Fig. 9b are color coded according to concurrently measured NO mixing ratios. The red open circles are average values of  $\text{OH}_{\text{obs}}/\text{OH}_{\text{mod}}$  over equally spaced  $\ln([\text{isoprene}]/\text{ppb})$  intervals for NO lower than 0.5 ppb. The error bars denote the variability within each NO interval. Panel (b): the averaged values from panel (a) (red open circles) are compared to  $\text{OH}_{\text{obs}}/\text{OH}_{\text{mod}}$  ratios reported from PROPHET (1998), INTEX (2004), GABRIEL (2006), and OP3-I (2008). Here, the error bars denote the stated measurement accuracies ( $2\sigma$ ) of OH.

a detailed isoprene chemistry and explicit ozonolysis of terpene (Tan et al., 2001) for PROPHET, MIM (Pöschl et al., 2000) for GABRIEL, and a lumped mechanism described by Crawford et al. (1999) for INTEX-A. For OP3, OH was calculated by an analytical equation with experimentally determined parameters under photostationary steady-state assumptions. The trend in Fig. 10b is apparently independent of the specific model used for OH prediction. It suggests that an OH source mechanism is missing in current models which is related to biogenic emissions or to their photochemical

daughter products. Anthropogenic VOCs made also a significant contribution to the OH reactivity at PRD (Lou et al., 2010), but their variability is too small to allow a positive identification of an influence on the OH model underprediction at PRD.

### 4.3 Model modifications to explain the observed HO<sub>x</sub>

#### 4.3.1 Additional radical recycling

In a previous study, Hofzumahaus et al. (2009) compared the experimental OH loss rate ( $k_{\text{OH}} \times [\text{OH}]$ ), calculated from measured concentrations and reactivities of OH, with the major known OH sources from photolysis of O<sub>3</sub> and HONO ( $P_{\text{OH}}$ ) and radical recycling ( $k_{\text{HO}_2+\text{NO}}[\text{NO}][\text{HO}_2]$ ) for PRIDE-PRD2006. The OH loss and production rates were found to be balanced in the morning when HO<sub>2</sub> was efficiently recycled to OH, but a significant OH source was missing in the afternoon at low NO. Several generic reaction pathways were tested that may explain the mismatch within the OH budget. In that paper, observed OH and HO<sub>2</sub> concentrations were utilized as target parameters for comparison with the model results. The most simple candidate for a new reaction pathway, which quantitatively explains the observations, was  $\text{RO}_2 + \text{X} \rightarrow \text{HO}_2$  in combination with  $\text{HO}_2 + \text{X} \rightarrow \text{OH}$  (Table 5, M1). This is the same type of reactions as those of peroxy-radicals with NO. Assuming rate constants as for the NO reactions, a concentration of 0.8 ppb was needed for X to match the mean diurnal profiles of both HO<sub>x</sub> species.

Since then, a strong interference in the HO<sub>2</sub> measurements by LIF from RO<sub>2</sub> was discovered (Fuchs et al., 2011, see Sect. 2.3). For this reason, the published results of the PRD campaign concerning the HO<sub>x</sub> budget have to be reevaluated. The previous major conclusion was that the recycling term  $k_{\text{HO}_2+\text{NO}}[\text{NO}][\text{HO}_2]$  in the OH budget was too small to explain the observed total OH loss rate. Since the interference of HO<sub>2</sub> by RO<sub>2</sub> has one direction, namely the enlargement of HO<sub>2</sub>\* with respect to the true HO<sub>2</sub>, the conclusion that additional OH recycling is missing in the model is still valid. Furthermore, the arguments made for the selection of the generic reaction terms with X still hold. However, a formerly excluded generic reaction type, a single reaction  $\text{HO}_2 + \text{Y} \rightarrow \text{OH}$  (Table 5, M2), has to be reconsidered. Before, M2 was ruled out, because the modelled HO<sub>2</sub> became much smaller than the measurement (HO<sub>2</sub>\*) when the simulated OH was matched to the observed OH. Since ambient HO<sub>2</sub> is smaller than HO<sub>2</sub>\* and we have no experimental constraint on RO<sub>2</sub>, results from model M2 can now be matched to the observations of both OH and HO<sub>2</sub>\*.

Figure 11 shows the mean diurnal variations of the modelled OH, HO<sub>2</sub>, HO<sub>2</sub>\* and RO<sub>2</sub> calculated by the RACM-MIM-GK model without (M0) and with additional radical recycling (M1, M2). The results for OH and HO<sub>2</sub>\* are also compared to the measured data. In case of M0, there is agree-

ment between modelled and measured OH in the morning, but a large discrepancy exists in the afternoon as discussed previously (Hofzumahaus et al., 2009). The modelled HO<sub>2</sub>\* is about 30 % larger than the modelled HO<sub>2</sub> and is in very good agreement with the measurement (HO<sub>2</sub>\*). Yet, even the modelled HO<sub>2</sub> is not significantly different from the measurement, given the combined experimental and model uncertainties (Hofzumahaus et al., 2009).

In model runs M1 and M2, the concentrations of the unknown reactants X and Y were optimized for half-hourly bins to achieve a best fit to the observed OH in the time interval 10:00–18:00 CNST (Fig. 11). Agreement is also achieved for modelled and measured HO<sub>2</sub>\* within the combined uncertainties. Thus, both types of additional recycling scenarios (M1, M2) provide acceptable generic solutions to describe the observed HO<sub>x</sub> data.

The effect of the additional recycling (M1, M2) on the OH chain length, defined as the ratio of the recycling rate ( $\text{HO}_2 \rightarrow \text{OH}$ ,  $\text{RO}_2 \rightarrow \text{OH}$ ) and  $P(\text{OH})$ , is to maintain the length at an almost constant value (about 10) during daytime, whereas the chain length drops to much lower values (1–2) in the afternoon if no additional recycling is assumed (Fig. S4).

Regarding the M1 case, the modelled HO<sub>2</sub>\* is about 30 % larger than the modelled HO<sub>2</sub> like in the base case (M0). In both cases, the RO<sub>2</sub>/HO<sub>2</sub> ratio is close to one and about half of the RO<sub>2</sub> species contribute significantly to the interference in the measured HO<sub>2</sub>. In the M2 calculation there is a huge difference of more than an order of magnitude between modelled HO<sub>2</sub> and HO<sub>2</sub>\*. The reason are very large calculated RO<sub>2</sub>/HO<sub>2</sub> ratios with values of 10–60 and corresponding ISOP/HO<sub>2</sub> ratios of 2–15 during the afternoon hours. The large difference of the RO<sub>2</sub>/HO<sub>2</sub> ratios between mechanism M1 and M2 would be a tool to distinguish which recycling type provides a more realistic description. However, experimental data of RO<sub>2</sub>/HO<sub>2</sub> ratios are not available for PRD and are also generally scarce in literature. In previous campaigns, Matrix Isolation Electron Spin Resonance (MIESR) has been applied to measure directly peroxy radicals in forested and suburban environments. RO<sub>2</sub>/HO<sub>2</sub> ratios were observed to vary from < 1 to 5 (Mihelcic et al., 2003). The ratio RO<sub>2</sub>/HO<sub>2</sub> has also been investigated by measurement techniques that apply chemical conversion, including LIF, peroxy radical chemical amplifiers (PERCA) and chemical ionization mass spectrometry (CIMS). Here, ratios of 4–15 were reported for a remote mountain site in Colorado (Stevens et al., 1997), < 1–9 for a rural area near Berlin (Platt et al., 2002), about 0.5 for a rural area in Pennsylvania (Ren et al., 2003), 1–3 for the free troposphere above Burkina Faso (Andrés-Hernández et al., 2010), about one for a remote mountain site in Italy (Hanke et al., 2002) and < 1–2 for the polluted outflow from Mexico City and Asian countries (Hornbrook et al., 2011). As reported by Fuchs et al. (2011) and Hornbrook et al. (2011), HO<sub>2</sub> measurement techniques like LIF or CIMS are susceptible to interferences from specific RO<sub>2</sub> radicals that are produced by atmospheric

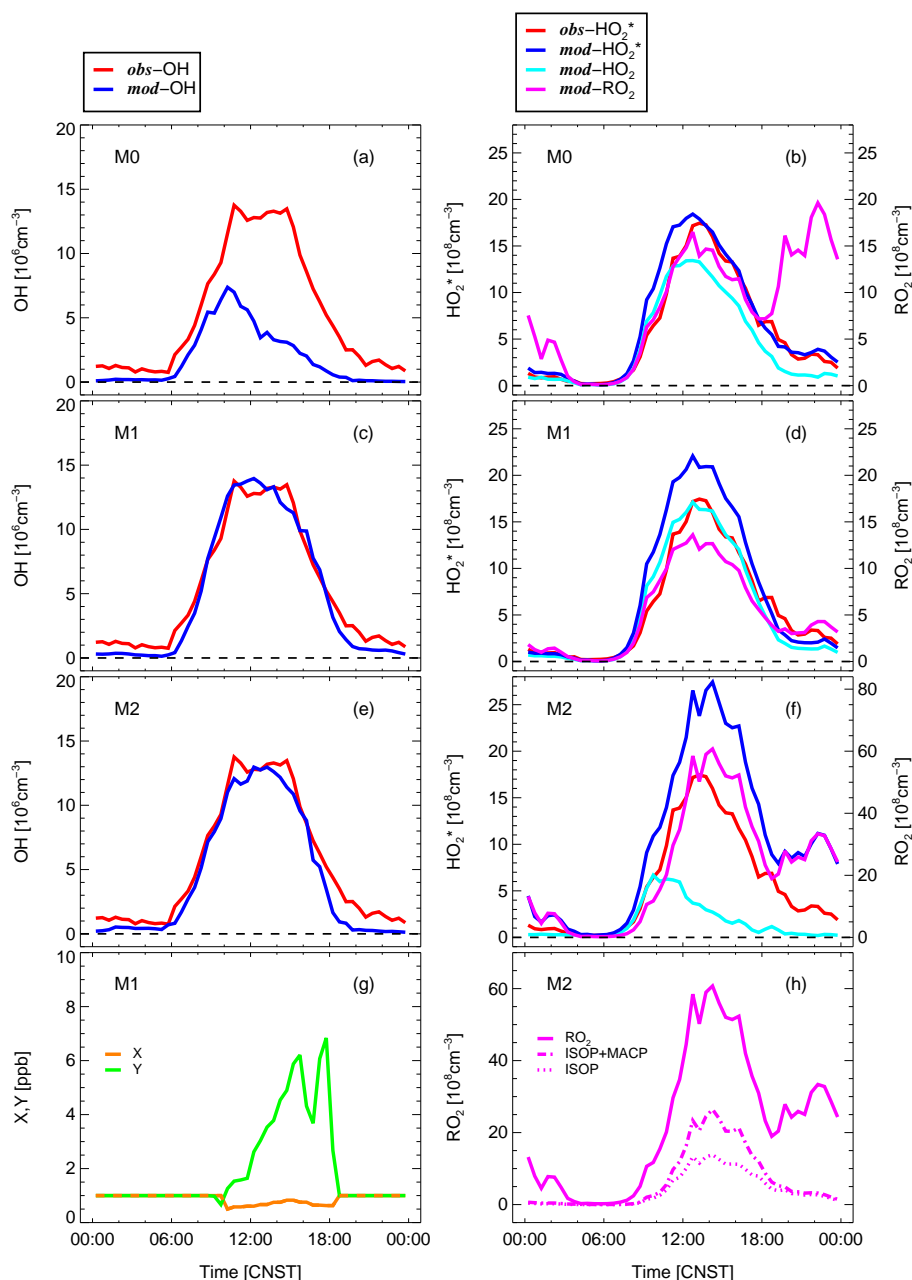


**Fig. 11.** Comparison of measured and modelled concentrations of OH and  $\text{HO}_2^*$  for three mechanistic scenarios (M0, M1 and M2). Panels (b), (d) and (f) show the modelled values of  $\text{HO}_2$  and  $\text{RO}_2$  as well. The fitted concentrations of the generic species X (scenario M1) and Y (scenario M2) are presented as NO equivalents in panel (g), and model results for peroxy radicals (ISOP, ISOP+MACP, total  $\text{RO}_2$ ) in panel (h).

oxidation of alkenes, dialkenes like isoprene, and aromatics. Thus, the reported  $\text{RO}_2/\text{HO}_2$  ratios determined by these techniques were probably underestimated. Furthermore, to our knowledge, the  $\text{RO}_2/\text{HO}_2$  ratio has never been determined experimentally for conditions like in this study with  $k_{\text{OH}}$  well above  $15 \text{ s}^{-1}$ . In conclusion, previously reported values of ambient  $\text{RO}_2/\text{HO}_2$ -ratios do not allow to choose between scenarios M1 and M2.

The proposed reactions with X or Y are the two most simple generic mechanisms that allow to reproduce the observed OH and  $\text{HO}_2^*$  concentrations. The reactions could either be real and involve an unidentified compound, or represent the overall effect of a more complex mechanism. Besides reactions of  $\text{HO}_2$  with organic species, which are investigated in Sect. 4.3.2, one could think of  $\text{HO}_2$  reactions with halogen oxides ( $\text{YO} = \text{BrO}$  or  $\text{IO}$ ). The influence of these species

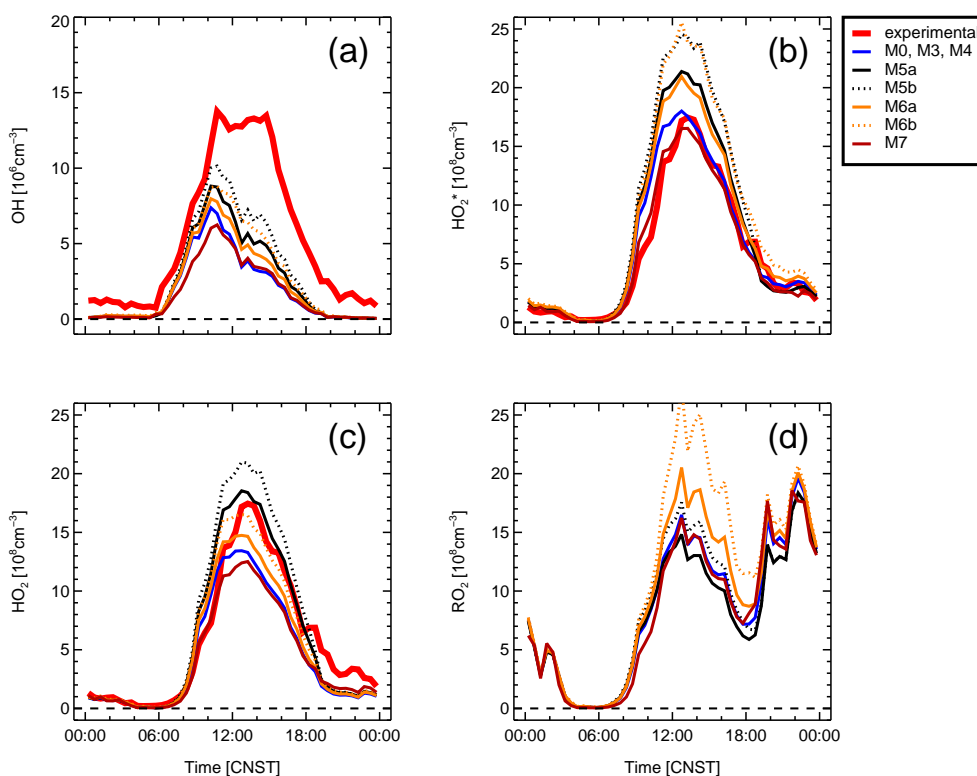


**Fig. 12.** Comparison of measured and modelled concentrations of OH (a) and HO<sub>2</sub><sup>\*</sup> (b), HO<sub>2</sub> (c), and RO<sub>2</sub> (d) for six different mechanistic scenarios: M0, M3, M4, M5a, M5b, M6, M7. The results for each radical species are not distinguishable among the model runs M0, M3 and M4 (differences are within the thickness of the lines).

on atmospheric HO<sub>x</sub> has been demonstrated for clean marine air (Read et al., 2008; Kanaya et al., 2007a; Bloss et al., 2005). For example, mean concentrations of 2.5 ppt BrO and 1.5 ppt IO observed at Cape Verde were found to enhance daytime OH by 5–12 % through the reactions HO<sub>2</sub> + YO → HOY + O<sub>2</sub> followed by HOY + *hν* → OH + Y (Read et al., 2008). The largest reported halogen oxide concentrations in the troposphere, 200 ppt BrO above the Dead Sea (Tas et al., 2005) and 20 ppt IO over sea-ice surfaces in coastal Antarctica (Saiz-Lopez et al., 2008) have HO<sub>2</sub> reactivities which correspond to 0.5 ppb and 0.2 ppb of NO, respectively. These values are too small compared to the required reactivities of X (equivalent of ~ 0.8 ppb NO) or Y (equivalent of ~ 5 ppb NO) displayed in Fig. 11. Since no particular halogen source was noted in PRD and as the required halogen oxide concentrations exceed all tropospheric observations, halogen oxide reactions are unlikely the missing OH source. Another speculative mechanism resembling HO<sub>2</sub> + Y → OH would be surface catalyzed conversion of HO<sub>2</sub> to OH on aerosols. This mechanism can be excluded due to the limitation in the HO<sub>2</sub> uptake as discussed further below (Sect. 4.3.3).

### 4.3.2 Mechanistic chemistry updates

As outlined in the introduction, a number of new chemical mechanisms have been proposed recently to explain the large model underprediction of OH observed in forested areas. Here, we test how well these OH regenerating mechanisms explain the discrepancy between modelled and measured OH at PRD. An overview of the tested mechanisms M3–M6 is given in Table 5. In addition, we show model results of the detailed MCMv3.1 (M7), which contains a more explicit description of the VOC chemistry compared to RACM-MIM-GK (M0). The corresponding model results for OH, HO<sub>2</sub>, HO<sub>2</sub><sup>\*</sup> and RO<sub>2</sub> and the measured OH and HO<sub>2</sub><sup>\*</sup> data are compared for M0 and M3–M7 in Fig. 12.

First we note that the results from MCMv3.1 (M7) agree well with the reference model (M0) especially at afternoon. This demonstrates that the OH underprediction by RACM-MIM-GK is not specifically caused by the lumped representation of the VOC chemistry, but is a fundamental deficit in our current understanding of tropospheric chemistry.

The implementation of additional OH formation from the reaction of HO<sub>2</sub> with acyl peroxy and β-keto peroxy radicals (Hasson et al., 2004; Jenkin et al., 2007; Dillon and Crowley, 2008) (M3) and with epoxide peroxy radicals (Paulot et al., 2009) (M4) has only a marginal impact on the modelled

concentrations of OH, HO<sub>2</sub>, HO<sub>2</sub><sup>\*</sup> and RO<sub>2</sub>. For each species, the modelled curves (Fig. 12) of the different scenarios M0, M3 and M4 are virtually indistinguishable. The reason for the small sensitivity to the RO<sub>2</sub> + HO<sub>2</sub> reactions is the dominating influence of the competing peroxy radical reactions with NO given average mixing ratios of more than 0.2 ppb NO at PRD.

The mechanisms M5 and M6 calculate significantly larger OH concentrations than M0. The model M5 includes the isoprene chemistry LIM0 postulated by Peeters and Müller (2010), whereas M6 contains additional OH formation by reaction of ISOP with HO<sub>2</sub> as proposed by Lelieveld et al. (2008) and Butler et al. (2008). Both mechanisms contain an “amplification” factor generating additional radicals within the radical recycling processes. In the LIM0 mechanism, amplification is achieved by the photolysis of HPALDs, which are assumed to have a yield of about one OH and one HO<sub>2</sub> (M5a), or alternatively up to three OH plus one HO<sub>2</sub> (M5b). The M6 scenario has two variants with yields of two (M6a) and four (M6b) OH radicals. Among the different M5 and M6 scenarios, M5b gives the largest increase of modelled OH by about a factor of two in the afternoon, relative to the M0 calculation. However, there is still a significant gap compared to the experimental data. The model explains only 40–50 % of the measured OH values during the afternoon at PRD, while it reproduces 70–90 % of the observed OH for the GABRIEL and INTEX-A campaigns (Stavrakou et al., 2010). In scenario M6b modelled OH increases on average by a factor of 1.7 in the afternoon, reaching only 30–40 % of the observed OH concentration. The same mechanism, however, was able to explain the GABRIEL and OP3-1 results by increasing the modelled OH by up to an order of magnitude (Lelieveld et al., 2008; Kubistin et al., 2010; Pugh et al., 2010). The different OH enhancements for PRIDE-PRD2006 and GABRIEL using M5b or M6b are caused by the different levels of NO, which were an order of magnitude larger at PRD compared to the Amazonian rain forest. At PRD, the competing peroxy radical reactions with NO decrease the sensitivity to radical amplification that is postulated in the mechanisms M5b and M6b. On the assumption that M5b and M6b represent mechanisms with maximum possible OH recycling efficiency from isoprene peroxy radicals, we may conclude that the unknown OH source at PRD is not solely connected to isoprene. There may be another, unidentified OH production mechanism which possibly involves oxidation products from other VOCs and/or unknown species X or Y.

The M5 and M6 scenarios calculate HO<sub>2</sub><sup>\*</sup> values that are larger than in the base case and overpredict the observed data by a factor 1.2–1.4. The modelled RO<sub>2</sub> is close to the corresponding HO<sub>2</sub> concentrations at daytime, so that the RO<sub>2</sub> to HO<sub>2</sub> ratio seems to be relatively independent of the chemical mechanisms used (M0, M3–M6). Table S8 in the Supplement shows that the relative contributions of speciated RO<sub>2</sub> radicals is not responding very much to changing OH con-

centrations. Thus, the difference between modelled HO<sub>2</sub> and HO<sub>2</sub><sup>\*</sup> is 20–40 % for M3–M6, close to the 30 % difference in M0.

The overprediction of HO<sub>2</sub><sup>\*</sup> is still within the model error of 40 %. Nevertheless, it could also be an indication that a sink process for peroxy radicals is missing in the model. In a similar case, Whalley et al. (2011) report an overprediction of HO<sub>2</sub> when they implement additional OH recycling in their model to explain OH observations in Borneo. They suppose that the mismatch between modelled and measured HO<sub>2</sub> points to a yet unknown additional HO<sub>2</sub> loss mechanism. A possible HO<sub>2</sub> sink, which is not included in our model runs (M0–M7), is heterogeneous loss on particles. The potential role of this process is discussed below.

#### 4.3.3 Heterogeneous radical loss

HO<sub>2</sub> radicals may be lost by heterogeneous uptake onto aerosol particles when competing gas-phase reactions of HO<sub>2</sub> are relatively slow. The potential influence of heterogeneous loss has been examined in model sensitivity studies mainly for marine environments (e.g. Carslaw et al., 1999, 2002; Sommariva et al., 2006; Kanaya et al., 2000, 2007a). Up to a factor of two of HO<sub>2</sub> reduction was simulated when the heterogeneous uptake coefficient for marine aerosol was assumed to be maximum,  $\gamma = 1$  (Sommariva et al., 2006; Kanaya et al., 2007a). During PRIDE-PRD2006, the daytime (08:00–18:00) averaged aerosol surface-area density was very large, about 1400  $\mu\text{m}^2 \text{cm}^{-3}$  (Li et al., 2011). The aerosol consisted mostly of submicron particles with an average particle-number size distribution peaking at a diameter of 100 nm (Yue et al., 2010). At such condition, uptake of HO<sub>2</sub> is reduced only little (about 10 %) by the resistance of diffusive gas transport. Assuming free molecular transport and  $\gamma = 0.5$ , the heterogeneous reactivity is calculated to be 0.1  $\text{s}^{-1}$  in comparison to 0.025  $\text{s}^{-1}$  by NO. Implementing this heterogeneous loss rate into model M0 causes a reduction of the calculated HO<sub>2</sub> by 50 %. This implies that a heterogeneous uptake process has the potential to reduce HO<sub>2</sub> at PRD significantly. However, the estimated strong influence is speculative. Though laboratory studies with Cu-II doped aqueous particles have shown large accommodation coefficients close to one (see overview, Kolb et al., 2010), measurements at salt solutions, soot and wet organic particles showed much smaller effective uptake coefficients in the range 0.01–0.1 (e.g. Thornton and Abbatt, 2005; Bedjanian et al., 2005; Taketani et al., 2009, 2010). Furthermore, the influence of heterogeneous uptake will be strongly diminished by competing HO<sub>2</sub> reactions which are required as additional OH sources (e.g. HO<sub>2</sub> + X). If HO<sub>2</sub> is heterogeneously lost, it will decrease the OH concentration as well. Alternatively, one could speculate about a heterogeneous reaction of HO<sub>2</sub> on particles that releases OH (or an OH precursor) into the gas-phase. However, the potential HO<sub>2</sub> reactivity towards aerosol is at least a factor of five too small

**Table 7.** Reaction rates (ppb h<sup>-1</sup>) and radical parameters averaged over the afternoon hours (12:00–16:00 CNST) from observation (Exp) and different model scenarios (M0–M7).

Reaction rate (ppb h <sup>-1</sup> )	Exp	M0	M1	M2	M3	M4	M5a	M5b	M6a	M6b	M7
<b>OH budget</b>											
$D(\text{OH})=[\text{OH}] \times k_{\text{OH}}$	34.1	10.4	46.3	40.9	11.0	11.0	15.6	21.8	14.4	21.5	9.7
$k_7[\text{HO}_2][\text{NO}]$	5.8 <sup>a</sup>	5.0	6.4	1.3	5.1	5.2	7.2	8.4	5.6	6.5	4.7
$2k_{13}[\text{O}^1\text{D}][\text{H}_2\text{O}]$	2.4	2.4	2.4	2.4	2.4	2.4	2.4	2.4	2.4	2.4	2.3
$j(\text{HONO})[\text{HONO}]$	0.9	0.9	0.9	0.9	0.9	0.9	0.9	0.9	0.9	0.9	0.9
$D(\text{OH})-P'(\text{OH})^b$	25.0 <sup>a</sup>	2.1	36.7	36.3	2.6	2.6	5.1	10.1	5.5	11.8	1.8
<b>Additional OH sources</b>											
$\text{HO}_2 + \text{X} \rightarrow \text{OH}$			33.7								
$\text{HO}_2 + \text{Y} \rightarrow \text{OH}$				34.4							
$\text{R}(\text{C}=\text{O})\text{R}'\text{O}_2 + \text{HO}_2 \rightarrow \text{OH}^c$					0.4	0.4	0.5	0.6	0.6	1.0	
$\text{IEPOXO}_2 + \text{HO}_2 \rightarrow \text{OH}^d$						0.1	0.1	0.1			
$\text{ISOP} \rightarrow \text{OH}^e$							0.3	0.5			
$\text{HPALDs} + h\nu \rightarrow m \times \text{OH}^e$							1.4	5.1			
$\text{ISOP} + \text{HO}_2 \rightarrow n \times \text{OH}^f$									2.2	7.1	
<b>Other reactions</b>											
$\text{ISOP} + \text{NO}$		0.9	0.9	4.1	0.9	1.0	0.3	0.4	1.1	1.5	1.0
$\text{HCHO} + h\nu \rightarrow 2 \times \text{HO}_2$		2.8	5.9	4.4	2.8	2.8	3.1	3.2	3.0	3.2	2.4
$\text{OVOCs} + h\nu \rightarrow \text{HO}_2^g$		0.7	1.6	1.3	0.7	0.7	2.2	2.6	0.8	1.0	0.6
<b>Ozone production</b>											
$P(\text{O}_3)$		10.7	11.3	19.9	10.9	10.7	12.5	14.7	12.4	15.1	10.7
$P(\text{O}_3)/([\text{OH}] \times k_{\text{OH}})$		1.0	0.2	0.5	1.0	1.0	0.8	0.7	0.9	0.7	1.1
<b>Radical parameters</b>											
$\text{OH} (10^6 \text{ cm}^{-3})$	12.6	3.1	12.2	11.8	3.3	3.4	4.8	6.3	4.1	5.6	3.3
$k_{\text{OH}} (\text{ s}^{-1})$	17.9	21.6	24.9	22.8	21.8	21.3	21.3	22.8	23.0	25.2	21.0
$\text{RO}_2/\text{HO}_2$		1.2	0.8	21.4	1.2	1.1	0.7	0.8	1.3	1.5	1.2
$\text{HO}_2/\text{OH}$	< 136 <sup>a</sup>	362	125	23	351	345	343	303	311	263	345

<sup>a</sup> Based on uncorrected HO<sub>2</sub><sup>\*</sup> values ( $[\text{HO}_2^*] > \text{HO}_2$ ); <sup>b</sup>  $P'(\text{OH}) = 2k_{13}[\text{O}^1\text{D}][\text{H}_2\text{O}] + j(\text{HONO})[\text{HONO}] + k_7[\text{HO}_2][\text{NO}]$ ; <sup>c</sup> R' = H or CH<sub>2</sub>, according to Taraborrelli et al. (2009); <sup>d</sup> According to Paulot et al. (2009); <sup>e</sup> According to Peeters and Müller (2010); <sup>f</sup> According to Lelieveld et al. (2008); <sup>g</sup> OVOCs without HCHO

compared the required reactivity to match the observed OH (cf. Fig. 11g, scenario M2). Thus, it seems unlikely that a surface-catalyzed HO<sub>2</sub> to OH recycling process is the missing OH source.

#### 4.3.4 OH radical budget analysis

Experimental and modelled (M0–M7) parameters that characterize the HO<sub>x</sub> chemistry during the afternoon hours 12:00–16:00 CNST at PRD are compared in Table 7. The main body of the table shows reaction rates that are relevant for the budget of OH and HO<sub>2</sub>, and the bottom gives radical parameters such as the mean concentration and reactivity of OH, as well as the RO<sub>2</sub>/HO<sub>2</sub> and HO<sub>2</sub>/OH ratios. It can be noted that the models M0 (RACM-MIM-GK), M3, M4 and M7 (MCMv3.1) yield almost identical values for each parameter, mostly within 10 %.

Following the OH budget analysis by Hofzumahaus et al. (2009), the total OH loss rate,  $D(\text{OH})$ , given by  $[\text{OH}] \times k_{\text{OH}}$  is compared to the total OH production rate,  $P'(\text{OH})$  (top of the table). Here,  $P'(\text{OH})$  is calculated from the photolysis of ozone and HONO, and from OH recycling by HO<sub>2</sub>+NO. Using solely experimental data, a missing OH source of about 25 ppb h<sup>-1</sup> is calculated. However, the recently detected interference in the HO<sub>2</sub> measurement introduces a systematic error. If the measured HO<sub>2</sub> data are corrected by –30 % as estimated by model M0, then the missing OH source is calculated to be 10 % larger, having a value of about 27 ppb h<sup>-1</sup>. If the measured HO<sub>2</sub> would be dominated by RO<sub>2</sub> (as predicted by model M2), then the missing OH source would have a 20 % larger value of at most 30 ppb h<sup>-1</sup>.

The models M0 and M7 show a small difference of about 2 ppb h<sup>-1</sup> between  $D(\text{OH})$  and  $P'(\text{OH})$  (Table 7), which is

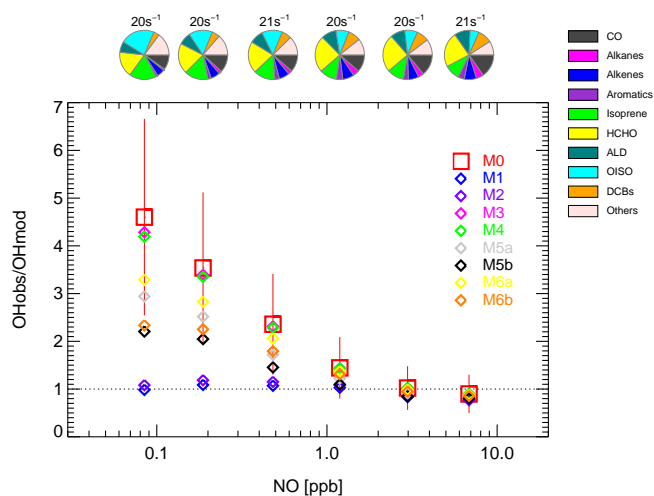


**Fig. 13.** NO dependence of the observed-to-modelled OH ratio ( $\text{OH}_{\text{obs}}/\text{OH}_{\text{mod}}$ ) for the different mechanistic scenarios M0 to M6 (see Table 5). Vertical error bars denote the combined  $1\sigma$  accuracies of the modelled (M0) and observed OH concentrations. Total VOC reactivities (M0 case) and their organic speciation (without  $\text{NO}_x$ ) are presented by pie charts at different NO intervals ( $\Delta \ln([\text{NO}]/\text{ppb}) = 0.17$ ) at the top. Abbrev. in the color legend of the pie charts: ALD = higher aldehydes than HCHO, OISO = MACR + MVK + CAR4, DCBs = MGLY + GLY + DCB, others = degradation products from hydrocarbons listed in Table 2 that exclude HCHO, ALD, OISO, DCBs.

caused by minor OH sources. These include ozonolysis of alkenes, photolysis of peroxides, OH recycling by  $\text{HO}_2 + \text{O}_3$  and prompt OH regeneration, e.g. from  $\text{ISHP} + \text{OH}$ . In case of the model scenarios M2–M6, the difference between  $D(\text{OH})$  and  $P'(\text{OH})$  is larger than in the base case (M0), owing to the additional OH sources implemented in each different mechanism. The respective source strengths are largest for M1 and M2, because they were fitted to match the observed OH. In the other models, the additional source strengths are not sufficient to match the observed OH. Models M3 and M4 have only marginal effects on the total OH production, whereas the scenarios M5b and M6b provide the most efficient additional OH sources among the newly proposed chemical mechanisms. It is interesting to note that the postulated OH formation from HPALD photolysis (M5b) is a factor of 1.6 more efficient than the corresponding photolysis of ozone and HONO. Since the HPALD photolysis is also expected to produce  $\text{HO}_2$  (Peeters and Müller, 2010), the contribution from HPALD photolysis to the  $\text{HO}_x$  radical pool would actually be larger than from the sum of photolysis rates of  $\text{O}_3$ , HONO, and HCHO.

#### 4.4 Further discussion

Two possible concepts have been discussed above to explain the difference between modelled (M0) and observed OH at

PRIDE-PRD2006. One concept introduces generic reactions with unknown species driving additional radical recycling (M1, M2). The other concept (M3–M6) relies on the implementation of newly discovered or proposed specific reactions that reproduce OH from peroxy radicals. The potential of each mechanism to explain the observed OH at PRD is compared in Fig. 13 as a function of NO at daytime conditions ( $j(\text{O}^1\text{D}) > 1 \times 10^{-5} \text{ s}^{-1}$ ). None of the mechanisms M3–M6 can reproduce the measured OH over the whole range of observed NO, whereas, not surprisingly, the generic mechanisms M1 and M2 show overall good agreement as a consequence of the numerical fitting of the unknown reactants X and Y. The spread among the model predictions is largest at the low end of the NO scale, where the newly implemented peroxy-radical reactions compete with different efficiencies with peroxy-peroxy radical termination reactions. As NO increases, the different model simulations converge, because peroxy radicals reactions with NO become dominant over the newly implemented reactions in the model mechanisms. At NO concentrations above 1 ppb, all mechanisms reproduce the measured OH reasonably well.

The observed NO dependence of the measured-to-modelled OH ratio (M0) is a new result that could be obtained at PRD due to the large variability of anthropogenic pollution in a rural area. Other studies at forest sites did not report such a NO dependence, probably because of the restricted NO range in (pristine) forests like in Amazonia (Lelieveld et al., 2008) or Borneo (Whalley et al., 2011). In fact, the NO concentrations there were generally smaller than the lowest NO values found at PRD. Contrary, the forest sites exhibited a large variability of (biogenic) VOCs, whereas the total VOC reactivity at PRD was rather constant ( $20 \text{ s}^{-1}$ ) during daytime with a moderate increase of isoprene by a factor of 1.6 from high (7 ppb) to low (0.08 ppb) values of NO (see reactivity data in Fig. 13).

Among the tested mechanisms, the additional recycling of OH from isoprene peroxy radicals in scenarios M5b and M6b offers the largest potential to bridge the gap between modelled (M0) and measured OH at low NO. Considering an estimated accuracy for  $\text{OH}_{\text{obs}}/\text{OH}_{\text{mod}}$  of 45 %, calculated by error propagation of the corresponding experimental and model uncertainties, the remaining discrepancy of a factor of two at  $\text{NO} < 0.2 \text{ ppb}$  is still significant. Apparently, the additional OH production in M5b or M6b is not efficient enough to explain the high OH concentrations at low NO. This may be due to uncertainties of the postulated mechanisms or to the relatively small amount of isoprene peroxy radicals which contribute only about 16 % of the modelled  $\text{RO}_2$  radicals (cf. Table S8 in the Supplement). A new laboratory study by Crouse et al. (2011) suggests that HPALD formation in the LIM0 mechanism is slower and the resulting OH recycling less efficient than originally proposed. Thus, besides OH recycling from isoprene peroxy radicals, another unidentified OH source must have been present at PRD, which may be possibly related to other VOCs besides isoprene. Further

laboratory studies are urgently needed to resolve this open question.

It is noteworthy that the unknown recycling mechanism (M1, M2) is also a requirement to explain the nighttime measurements of OH and HO<sub>2</sub><sup>\*</sup>, which had mean values of  $2 \times 10^6 \text{ cm}^{-3}$  and  $2 \times 10^8 \text{ cm}^{-3}$ , respectively. The base model (M0) can explain HO<sub>2</sub><sup>\*</sup> from ozonolysis, but strongly underestimates the measured OH levels. In order to explain both OH and HO<sub>2</sub><sup>\*</sup> at night, an additional recycling process like at daytime is needed and a small additional primary source of OH which would be negligible during daytime. Details of this analysis will be presented elsewhere (Lu et al., 2012).

We have recently tested our LIF instrument for possible measurement artifacts in VOC and isoprene rich air at PRD-like conditions in the atmosphere simulation chamber SAPHIR in Jülich by comparison with an open-path OH-DOAS (differential optical absorption spectroscopy) instrument. Like in previous intercomparisons (Hofzumahaus et al., 1998; Schlosser et al., 2006, 2009) we find no indication of a significant measurement interference in LIF that could explain the high OH values observed at PRD.

The proposed additional OH sources in M1–M6 all rely on radical recycling without oxidation of NO to NO<sub>2</sub>. Thus, they do not contribute to photochemical ozone formation. This is reflected by the  $P(\text{O}_3)/[\text{OH}] \times k_{\text{OH}}$  ratio (Table 7), where  $P(\text{O}_3)$  denotes the ozone production rate from the reactions of HO<sub>2</sub> and RO<sub>2</sub> with NO. While the established mechanism M0 and M7 predict a ratio of one for the conditions at PRD, a strongly reduced ozone production efficiency is expected from M1 and M2. In case of the scenarios M5b and M6b, a reduction of 30 % is calculated. The large variability of the calculated ozone production efficiency between the different mechanisms demonstrates that the insufficient understanding of the radical recycling mechanism also introduces a significant uncertainty in the predictions of secondary pollutants.

## 5 Summary and conclusions

Ambient OH and HO<sub>2</sub> concentrations were measured by LIF during the PRIDE-PRD2006 campaign at a rural site downwind of Guangzhou in the Pearl River Delta in summer 2006. The most obvious feature of the HO<sub>x</sub> photochemistry for this campaign was published by Hofzumahaus et al. (2009). A large imbalance between the experimentally determined total OH loss rate and production of OH from known radical sources was discovered, indicating a missing OH source at conditions of high isoprene (2 ppb) and low NO (0.1–0.2 ppb). A generic reaction pathway, RO<sub>2</sub> + X → HO<sub>2</sub> and HO<sub>2</sub> + X → OH was proposed to enable a chemical model to reproduce both the observed OH and HO<sub>2</sub> concentrations. In this work, we have reevaluated the dataset and extended the model analysis, taking into account a newly discovered

artefact in the LIF measurement of HO<sub>2</sub>. The major findings are:

1. Considering the interference from RO<sub>2</sub> in the HO<sub>2</sub> detection channel, the need for an additional HO<sub>2</sub> → OH recycling process persists. Since the true HO<sub>2</sub> concentration is smaller than the measured value HO<sub>2</sub><sup>\*</sup>, the missing OH source may be up to 85 % of the OH loss rate rather than 74 % calculated previously. Moreover, the need of an adjacent recycling RO<sub>2</sub> → HO<sub>2</sub> to match the observed HO<sub>2</sub> has diminished, since the measured HO<sub>2</sub> data contain a contribution from RO<sub>2</sub> that is not known quantitatively. The concentrations of individual RO<sub>2</sub> species would be needed for a correction of the interference which is not attainable in retrospect.
2. Daily maxima of OH and HO<sub>2</sub><sup>\*</sup> were in the range of  $(15\text{--}26) \times 10^6 \text{ cm}^{-3}$  and  $(3\text{--}25) \times 10^8 \text{ cm}^{-3}$ , respectively. Compared to previously reported measurements in other urban and suburban areas, the OH concentrations at PRD are among the highest values so far reported. Measured HO<sub>2</sub> concentrations reported in the literature are difficult to compare, because they were obtained by LIF techniques and likely influenced by unspecified interferences from RO<sub>2</sub> similar to our case.
3. The observed OH showed a consistent high correlation with  $j(\text{O}^1\text{D})$  over a broad range of NO<sub>x</sub> conditions. The correlation cannot be reproduced by model simulations, indicating that OH stabilizing processes are missing in current models (e.g. RACM-MIM-GK).
4. The observed OH exhibited only a weak dependence on NO<sub>x</sub> in contrast to model predictions. While modelled and measured OH agree well at NO mixing ratios above 1 ppb, a continuously increasing underprediction of the observed OH is found towards lower NO concentrations, reaching a factor of 8 at 0.02 ppb NO.
5. A dependence of the modelled-to-measured OH ratio on isoprene cannot be derived from the PRD data set due to the relatively small isoprene variability. However, the magnitude of the ratio fits into the isoprene dependent trend that was reported from other campaigns in forested regions.
6. Two recently postulated isoprene mechanisms (Lelieveld et al., 2008; Peeters and Müller, 2010) lead to significant enhancements of OH expected for PRD, but an underprediction of the observed OH by a factor of 2 remains at low NO. If the photolysis of HPALDs is as efficient as proposed in the LIM0 mechanism by Peeters and Müller (2010), the corresponding OH formation at PRD would be more important than the primary OH production from ozone and HONO.

The isoprene mechanisms by Lelieveld et al. (2008) and Peeters and Müller (2010) have shown potential to explain



the unexpectedly large OH concentrations observed above forests during the GABRIEL and INTEX-A campaigns. The still significant underprediction of OH at the NO concentration regime of PRD may be explained either by the uncertainties of the postulated mechanisms which are not yet confirmed by laboratory studies, or by other so far unidentified OH sources that may have played a role. Further experimental investigations will be needed to get a full picture of the radical chemistry in VOC rich environments. Improved measurement techniques for HO<sub>2</sub> and (speciated) RO<sub>2</sub> would be extremely helpful in future studies to gain more insight into the cycling of radicals and its impact on tropospheric photochemistry.

**Supplementary material related to this article is available online at:**

<http://www.atmos-chem-phys.net/12/1541/2012/acp-12-1541-2012-supplement.pdf>

*Acknowledgements.* We thank the PRIDE-PRD2006 campaign team (2002CB410801), especially F. Yang, H. Su, A. Nowak, N. Takegawa, and A. Oebel for help and support at the field site. We thank P. H. Xie, Anhui Institute of Optics and Fine Mechanics in Hefei, China, for providing the methane data. We acknowledge financial support by the National Natural Science Foundation of China (Major Program: 21190052) and by EU-project PEGASOS (grant no. 265307).

Edited by: A. Wiedensohler

## References

- Andrés-Hernández, M. D., Stone, D., Brookes, D. M., Commane, R., Reeves, C. E., Huntrieser, H., Heard, D. E., Monks, P. S., Burrows, J. P., Schlager, H., Kartal, D., Evans, M. J., Floquet, C. F. A., Ingham, T., Methven, J., and Parker, A. E.: Peroxy radical partitioning during the AMMA radical intercomparison exercise, *Atmos. Chem. Phys.*, 10, 10621–10638, doi:10.5194/acp-10-10621-2010, 2010.
- Archibald, A. T., Cooke, M. C., Utembe, S. R., Shallcross, D. E., Derwent, R. G., and Jenkin, M. E.: Impacts of mechanistic changes on HO<sub>x</sub> formation and recycling in the oxidation of isoprene, *Atmos. Chem. Phys.*, 10, 8097–8118, doi:10.5194/acp-10-8097-2010, 2010.
- Atkinson, R.: Atmospheric reactions of alkoxy and β-hydroxyalkoxy radicals, *Int. J. Chem. Kin.*, 29, 99–111, 1997.
- Bedjanian, Y., Lelievre, S., and Le Bras, G.: Experimental study of the interaction of HO<sub>2</sub> radicals with soot surface, *Phys. Chem. Chem. Phys.*, 7, 334–341, 2005.
- Berresheim, H., Plass-Dülmer, C., Elste, T., Mihalopoulos, N., and Rohrer, F.: OH in the coastal boundary layer of Crete during MINOS: Measurements and relationship with ozone photolysis, *Atmos. Chem. Phys.*, 3, 639–649, doi:10.5194/acp-3-639-2003, 2003.
- Bloss, W. J., Lee, J. D., Johnson, G. P., Sommariva, R., Heard, D. E., Saiz-Lopez, A., Plane, J. M. C., McFiggans, G., Coe, H., Flynn, M., Williams, P., Rickard, A. R., and Fleming, Z. L.: Impact of halogen monoxide chemistry upon boundary layer OH and HO<sub>2</sub> concentrations at a coastal site, *Geophys. Res. Lett.*, 32, L06814, doi:10.1029/2004GL022084, 2005.
- Bohn, B., Corlett, G. K., Gillmann, M., Sanghavi, S., Stange, G., Tensing, E., Vrekoussis, M., Bloss, W. J., Clapp, L. J., Kortner, M., Dorn, H.-P., Monks, P. S., Platt, U., Plass-Dülmer, C., Mihalopoulos, N., Heard, D. E., Clemmshaw, K. C., Meixner, F. X., Prevot, A. S. H., and Schmitt, R.: Photolysis frequency measurement techniques: results of a comparison within the ACCENT project, *Atmos. Chem. Phys.*, 8, 5373–5391, doi:10.5194/acp-8-5373-2008, 2008.
- Brasseur, G. P., Prinn, R. G., and Pszenny, A. P. (Eds.): *Atmospheric Chemistry in a Changing World*, The IGBP Series, Springer, Berlin, 2003.
- Brauers, T., Hausmann, M., Bister, A., Kraus, A., and Dorn, H. P.: OH radicals in the boundary layer of the Atlantic Ocean 1. Measurements by long-path laser absorption spectroscopy, *J. Geophys. Res.*, 106, 7399–7414, 2001.
- Butler, T. M., Taraborrelli, D., Brühl, C., Fischer, H., Harder, H., Martinez, M., Williams, J., Lawrence, M. G., and Lelieveld, J.: Improved simulation of isoprene oxidation chemistry with the ECHAM5/MESy chemistry-climate model: lessons from the GABRIEL airborne field campaign, *Atmos. Chem. Phys.*, 8, 4529–4546, doi:10.5194/acp-8-4529-2008, 2008.
- Carslaw, N., Creasey, D. J., Heard, D. E., Lewis, A. C., McQuaid, J. B., Pilling, M. J., Monks, P. S., Bandy, B. J., and Penkett, S. A.: Modeling OH, HO<sub>2</sub>, and RO<sub>2</sub> radicals in the marine boundary layer – 1. Model construction and comparison with field measurements, *J. Geophys. Res.*, 104, 30241–30255, 1999.
- Carslaw, N., Creasey, D., Heard, D., Jacobs, P., Lee, J., Lewis, A., Bauguitte, S., Penkett, S., Monks, P., and Salisbury, G.: Eastern Atlantic Spring Experiment 1997 (EASE97) 2. Comparisons of model concentrations of OH, HO<sub>2</sub>, and RO<sub>2</sub> with measurements, *J. Geophys. Res.*, 107, 4190, doi:10.1029/2001JD001568, 2002.
- Chan, C. K. and Yao, X.: Air pollution in mega cities in China, *Atmos. Environ.*, 42, 1–42, 2008.
- Crawford, J., Davis, D., Olson, J., Chen, G., Liu, S., Gregory, G., Barrick, J., Sachse, G., Sandholm, S., Heikes, B., Singh, H., and Blake, D.: Assessment of upper tropospheric HO<sub>x</sub> sources over the tropical Pacific based on NASA GTE/PEM data: Net effect on HO<sub>x</sub> and other photochemical parameters, *J. Geophys. Res.*, 104, 16255–16273, 1999.
- Creasey, D. J., Heard, D. E., and Lee, J. D.: Eastern Atlantic Spring Experiment 1997 (EASE97) 1. Measurements of OH and HO<sub>2</sub> concentrations at Mace Head, Ireland, *J. Geophys. Res.*, 107, D104091, doi:10.1029/2001JD000892, 2002.
- Crosley, D. R.: The measurement of OH and HO<sub>2</sub> in the atmosphere, *J. Atmos. Sci.*, 52, 3299–3314, 1995.
- Crouse, J. D., Paulot, F., Kjaergaard, H. G., and Wennberg, P. O.: Peroxy radical isomerization in the oxidation of isoprene, *Phys. Chem. Chem. Phys.*, 13, 13607–13613, doi:10.1039/c1cp21330j, 2011.
- Dillon, T. J. and Crowley, J. N.: Direct detection of OH formation in the reactions of HO<sub>2</sub> with CH<sub>3</sub>C(O)O<sub>2</sub> and other substituted peroxy radicals, *Atmos. Chem. Phys.*, 8, 4877–4889, doi:10.5194/acp-8-4877-2008, 2008.
- Dusanter, S., Vimal, D., Stevens, P. S., Volkamer, R., Molina, L. T., Baker, A., Meinardi, S., Blake, D., Sheehy, P., Merten, A.,

- Zhang, R., Zheng, J., Fortner, E. C., Junkermann, W., Dubey, M., Rahn, T., Eichinger, B., Lewandowski, P., Prueger, J., and Holder, H.: Measurements of OH and HO<sub>2</sub> concentrations during the MCMA-2006 field campaign – Part 2: Model comparison and radical budget, *Atmos. Chem. Phys.*, 9, 6655–6675, doi:10.5194/acp-9-6655-2009, 2009.
- Ehhalt, D. H.: Photooxidation of trace gases in the troposphere, *Phys. Chem. Chem. Phys.*, 1, 5401–5408, 1999.
- Ehhalt, D. H. and Rohrer, F.: Dependence of the OH concentration on solar UV, *J. Geophys. Res.*, 105, 3565–3571, 2000.
- Emmerson, K. M., Carslaw, N., Carpenter, L. J., Heard, D. E., Lee, J. D., and Pilling, M. J.: Urban atmospheric chemistry during the PUMA campaign 1: Comparison of modelled OH and HO<sub>2</sub> concentrations with measurements, *J. Atmos. Chem.*, 52, 143–164, 2005.
- Emmerson, K. M., Carslaw, N., Carslaw, D. C., Lee, J. D., McFiggans, G., Bloss, W. J., Gravestock, T., Heard, D. E., Hopkins, J., Ingham, T., Pilling, M. J., Smith, S. C., Jacob, M., and Monks, P. S.: Free radical modelling studies during the UK TORCH Campaign in Summer 2003, *Atmos. Chem. Phys.*, 7, 167–181, doi:10.5194/acp-7-167-2007, 2007.
- Finlayson-Pitts, B. J. and Pitts Jr., J. N.: *Chemistry of the upper and lower atmosphere: Theory, experiments and applications*, Academic Press, San Diego, 2000.
- Fuchs, H., Bohn, B., Hofzumahaus, A., Holland, F., Lu, K. D., Nehr, S., Rohrer, F., and Wahner, A.: Detection of HO<sub>2</sub> by laser-induced fluorescence: calibration and interferences from RO<sub>2</sub> radicals, *Atmos. Meas. Tech.*, 4, 1209–1225, doi:10.5194/amt-4-1209-2011, 2011.
- Garland, R. M., Yang, H., Schmid, O., Rose, D., Nowak, A., Achtert, P., Wiedensohler, A., Takegawa, N., Kita, K., Miyazaki, Y., Kondo, Y., Hu, M., Shao, M., Zeng, L. M., Zhang, Y. H., Andreae, M. O., and Pöschl, U.: Aerosol optical properties in a rural environment near the mega-city Guangzhou, China: implications for regional air pollution, radiative forcing and remote sensing, *Atmos. Chem. Phys.*, 8, 5161–5186, doi:10.5194/acp-8-5161-2008, 2008.
- Geiger, H., Barnes, I., Bejan, I., Benter, T., and Spittler, M.: The tropospheric degradation of isoprene: an updated module for the regional atmospheric chemistry mechanism, *Atmos. Environ.*, 37, 1503–1519, 2003.
- George, L. A., Hard, T. M., and O'Brien, R. J.: Measurement of free radicals OH and HO<sub>2</sub> in Los Angeles smog, *J. Geophys. Res.*, 104, 11643–11655, 1999.
- Hallquist, M., Wenger, J. C., Baltensperger, U., Rudich, Y., Simpson, D., Claeys, M., Dommen, J., Donahue, N. M., George, C., Goldstein, A. H., Hamilton, J. F., Herrmann, H., Hoffmann, T., Iinuma, Y., Jang, M., Jenkin, M. E., Jimenez, J. L., Kiendler-Scharr, A., Maenhaut, W., McFiggans, G., Mentel, Th. F., Monod, A., Prévôt, A. S. H., Seinfeld, J. H., Surratt, J. D., Szmigielski, R., and Wildt, J.: The formation, properties and impact of secondary organic aerosol: current and emerging issues, *Atmos. Chem. Phys.*, 9, 5155–5236, doi:10.5194/acp-9-5155-2009, 2009.
- Hanke, M., Uecker, J., Reiner, T., and Arnold, F.: Atmospheric peroxy radicals: ROXMAS, a new mass-spectrometric methodology for speciated measurements of HO<sub>2</sub> and ΣRO<sub>2</sub> and first results, *Int. J. Mass Spectrom.*, 213, 91–99, 2002.
- Harrison, R. M., Yin, J., Tilling, R. M., Cai, X., Seakins, P. W., Hopkins, J. R., Lansley, D. L., Lewis, A. C., Hunter, M. C., Heard, D. E., Carpenter, L. J., Creasey, D. J., Lee, J. D., Pilling, M. J., Carslaw, N., Emmerson, K. M., Redington, A., Derwent, R. G., Ryall, D., Mills, G., and Penkett, S. A.: Measurement and modelling of air pollution and atmospheric chemistry in the U.K. West Midlands conurbation: Overview of the PUMA Consortium project, *Sci. Total. Environ.*, 360, 5–25, 2006.
- Hasson, A. S., Tyndall, G. S., and Orlando, J. J.: A product yield study of the reaction of HO<sub>2</sub> radicals with ethyl peroxy (C<sub>2</sub>H<sub>5</sub>O<sub>2</sub>), acetyl peroxy (CH<sub>3</sub>C(O)O<sub>2</sub>), and acetonyl peroxy (CH<sub>3</sub>C(O)CH<sub>2</sub>O<sub>2</sub>) radicals, *J. Phys. Chem. A*, 108, 5979–5989, 2004.
- Heard, D. E. and Pilling, M. J.: Measurement of OH and HO<sub>2</sub> in the Troposphere, *Chem. Rev.*, 103, 5163–5198, 2003.
- Hofzumahaus, A., Aschmutat, U., Heßling, M., Holland, F., and Ehhalt, D. H.: The measurement of tropospheric OH radicals by laser-induced fluorescence spectroscopy during the POPCORN field campaign, *Geophys. Res. Lett.*, 23, 2541–2544, 1996.
- Hofzumahaus, A., Aschmutat, U., Brandenburger, U., Brauers, T., Dorn, H.-P., Hausmann, M., Hessling, M., Holland, F., Plass-Dülmer, C., and Ehhalt, D. H.: Intercomparison of tropospheric OH measurements by different laser techniques during the POPCORN Campaign 1994, *J. Atmos. Chem.*, 31, 227–246, 1998.
- Hofzumahaus, A., Rohrer, F., Lu, K., Bohn, B., Brauers, T., Chang, C. C., Fuchs, H., Holland, F., Kita, K., Kondo, Y., Li, X., Lou, S., Shao, M., Zeng, L., Wahner, A., and Zhang, Y.: Amplified Trace Gas Removal in the Troposphere, *Science*, 324, 1702–1704, 2009.
- Holland, F., Heßling, M., and Hofzumahaus, A.: In situ measurement of tropospheric OH radicals by laser-induced fluorescence – A description of the KFA instrument, *J. Atmos. Sci.*, 52, 3393–3401, 1995.
- Holland, F., Aschmutat, U., Heßling, M., Hofzumahaus, A., and Ehhalt, D. H.: Highly time resolved measurements of OH during POPCORN using laser-induced fluorescence spectroscopy, *J. Atmos. Chem.*, 31, 205–225, 1998.
- Holland, F., Hofzumahaus, A., Schäfer, J., Kraus, A., and Pätz, H.-W.: Measurements of OH and HO<sub>2</sub> radical concentrations and photolysis frequencies during BERLIOZ, *J. Geophys. Res.*, 108, 8246, doi:10.1029/2001JD001393, 2003.
- Hornbrook, R. S., Crawford, J. H., Edwards, G. D., Goyea, O., Mauldin III, R. L., Olson, J. S., and Cantrell, C. A.: Measurements of tropospheric HO<sub>2</sub> and RO<sub>2</sub> by oxygen dilution modulation and chemical ionization mass spectrometry, *Atmos. Meas. Tech.*, 4, 735–756, doi:10.5194/amt-4-735-2011, 2011.
- Jenkin, M. E., Saunders, S. M., Wagner, V., and Pilling, M. J.: Protocol for the development of the Master Chemical Mechanism, MCM v3 (Part B): tropospheric degradation of aromatic volatile organic compounds, *Atmos. Chem. Phys.*, 3, 181–193, doi:10.5194/acp-3-181-2003, 2003.
- Jenkin, M. E., Hurley, M. D., and Wallington, T. J.: Investigation of the radical product channel of the CH<sub>3</sub>C(O)O<sub>2</sub>+HO<sub>2</sub> reaction in the gas phase, *Phys. Chem. Chem. Phys.*, 9, 3149–3162, 2007.
- Jenkin, M. E., Hurley, M. D., and Wallington, T. J.: Investigation of the radical product channel of the CH<sub>3</sub>OCH<sub>2</sub>O<sub>2</sub> + HO<sub>2</sub> reaction in the gas phase, *J. Phys. Chem. A*, 114, 408–416, 2010.
- Kanakidou, M., Seinfeld, J. H., Pandis, S. N., Barnes, I., Dentener, F. J., Facchini, M. C., Van Dingenen, R., Ervens, B., Nenes, A., Nielsen, C. J., Swietlicki, E., Putaud, J. P., Balkanski, Y., Fuzzi,

- S., Horth, J., Moortgat, G. K., Winterhalter, R., Myhre, C. E. L., Tsigaridis, K., Vignati, E., Stephanou, E. G., and Wilson, J.: Organic aerosol and global climate modelling: a review, *Atmos. Chem. Phys.*, 5, 1053–1123, doi:10.5194/acp-5-1053-2005, 2005.
- Kanaya, Y., Sadanaga, Y., Matsumoto, J., Sharma, U. K., Hirokawa, J., Kajii, Y., and Akimoto, H.: Daytime HO<sub>2</sub> concentrations at Oki Island, Japan, in summer 1998: Comparison between measurement and theory, *J. Geophys. Res.*, 105, 24205–24222, 2000.
- Kanaya, Y., Sadanaga, Y., Hirokawa, J., Kajii, Y., and Akimoto, H.: Development of a ground-based LIF instrument for measuring HO<sub>x</sub> radicals: Instrumentation and calibrations, *J. Atmos. Chem.*, 38, 73–110, 2001.
- Kanaya, Y., Cao, R., Kato, S., Miyakawa, Y., Kajii, Y., Tanimoto, H., Yokouchi, Y., Mochida, M., Kawamura, K., and Akimoto, H.: Chemistry of OH and HO<sub>2</sub> radicals observed at Rishiri Island, Japan, in September 2003: Missing daytime sink of HO<sub>2</sub> and positive nighttime correlations with monoterpenes, *J. Geophys. Res.*, 112, D11308, doi:10.1029/2006JD007987, 2007a.
- Kanaya, Y., Cao, R. Q., Akimoto, H., Fukuda, M., Komazaki, Y., Yokouchi, Y., Koike, M., Tanimoto, H., Takegawa, N., and Kondo, Y.: Urban photochemistry in central Tokyo: 1. Observed and modeled OH and HO<sub>2</sub> radical concentrations during the winter and summer of 2004, *J. Geophys. Res.*, 112, D21312, doi:10.1029/2007JD008670, 2007b.
- Karl, M., Dorn, H.-P., Holland, F., Koppmann, R., Poppe, D., Rupp, L., Schaub, A., and Wahner, A.: Product study of the reaction of OH radicals with isoprene in the atmosphere simulation chamber SAPHIR, *J. Atmos. Chem.*, 55, 167–187, 2006.
- Kleffmann, J., Gavriloaiei, T., Hofzumahaus, A., Holland, F., Koppmann, R., Rupp, L., Schlosser, E., Siese, M., and Wahner, A.: Daytime formation of nitrous acid: A major source of OH radicals in a forest, *Geophys. Res. Lett.*, 32, L05818, doi:10.1029/2005GL022524, 2005.
- Kolb, C. E., Cox, R. A., Abbatt, J. P. D., Ammann, M., Davis, E. J., Donaldson, D. J., Garrett, B. C., George, C., Griffiths, P. T., Hanson, D. R., Kulmala, M., McFiggans, G., Pöschl, U., Riipinen, I., Rossi, M. J., Rudich, Y., Wagner, P. E., Winkler, P. M., Worsnop, D. R., and O' Dowd, C. D.: An overview of current issues in the uptake of atmospheric trace gases by aerosols and clouds, *Atmos. Chem. Phys.*, 10, 10561–10605, doi:10.5194/acp-10-10561-2010, 2010.
- Kubistin, D., Harder, H., Martinez, M., Rudolf, M., Sander, R., Bozem, H., Eerdeken, G., Fischer, H., Gurk, C., Klüpfel, T., Königstedt, R., Parchatka, U., Schiller, C. L., Stickler, A., Taraborrelli, D., Williams, J., and Lelieveld, J.: Hydroxyl radicals in the tropical troposphere over the Suriname rainforest: comparison of measurements with the box model MECCA, *Atmos. Chem. Phys.*, 10, 9705–9728, doi:10.5194/acp-10-9705-2010, 2010.
- Lelieveld, J., Butler, T. M., Crowley, J. N., Dillon, T. J., Fischer, H., Ganzeveld, L., Harder, H., Lawrence, M. G., Martinez, M., Taraborrelli, D., and Williams, J.: Atmospheric oxidation capacity sustained by a tropical forest, *Nature*, 452, 737–740, 2008.
- Lewis, A. C., Hopkins, J. R., Carpenter, L. J., Stanton, J., Read, K. A., and Pilling, M. J.: Sources and sinks of acetone, methanol, and acetaldehyde in North Atlantic marine air, *Atmos. Chem. Phys.*, 5, 1963–1974, doi:10.5194/acp-5-1963-2005, 2005.
- Li, S. P., Matthews, J., and Sinha, A.: Atmospheric hydroxyl radical production from electronically excited NO<sub>2</sub> and H<sub>2</sub>O, *Science*, 319, 1657–1660, 2008.
- Li, X., Brauers, T., Hofzumahaus, A., Lu, K., Li, Y. P., Shao, M., Wagner, T., and Wahner, A.: MAX-DOAS measurements of NO<sub>2</sub>, HCHO and CHOCHO at a rural site in Southern China, *Atmos. Chem. Phys. Discuss.*, 12, 3983–4029, doi:10.5194/acpd-12-3983-2012, 2012.
- Li, X., Brauers, T., Häsel, R., Bohn, B., Hofzumahaus, A., Holland, F., Lu, K. D., Rohrer, F., Hu, M., Zeng, L. M., Zhang, Y. H., Garland, R., Su, H., Nowak, A., Takegawa, N., Shao, M., and Wahner, A.: Exploring the atmospheric chemistry of nitrous acid (HONO) at a rural site in Southern China, *Atmos. Chem. Phys. Discuss.*, 11, 27591–27635, doi:10.5194/acpd-11-27591-2011, 2011.
- Lou, S., Holland, F., Rohrer, F., Lu, K., Bohn, B., Brauers, T., Chang, C., Fuchs, H., Häsel, R., Kita, K., Kondo, Y., Li, X., Shao, M., Zeng, L., Wahner, A., Zhang, Y., Wang, W., and Hofzumahaus, A.: Atmospheric OH reactivities in the Pearl River Delta – China in summer 2006: measurement and model results, *Atmos. Chem. Phys.*, 10, 11243–11260, doi:10.5194/acp-10-11243-2010, 2010.
- Lu, K. D., Zhang, Y. H., Su, H., Shao, M., Zeng, L. M., Zhong, L. J., Xiang, Y. R., Chang, C. C., Chou, C. K. C., and Wahner, A.: Regional ozone pollution and key controlling factors of photochemical ozone production in Pearl River Delta during summer time, *Sci. China, Ser. B*, 53, 651–663, 2010.
- Lu, K. D., Rohrer, F., Hofzumahaus, A., et al.: Nighttime HO<sub>x</sub> chemistry in the Pearl River Delta and Beijing in summer 2006, *Atmos. Chem. Phys. Discuss.*, in preparation, 2012.
- Mao, J., Ren, X., Chen, S., Brune, W. H., Chen, Z., Martinez, M., Harder, H., Lefter, B., Rappenglück, B., Flynn, J., and Leuchner, M.: Atmospheric oxidation capacity in the summer of Houston 2006: Comparison with summer measurements in other metropolitan studies, *Atmos. Environ.*, 44, 4107–4115, doi:10.1016/j.atmosenv.2009.01.013, 2010.
- Martinez, M., Harder, H., Kovacs, T. A., Simpas, J. B., Bassis, J., Leshner, R., Brune, W. H., Frost, G. J., Williams, E. J., Stroud, C. A., Jobson, B. T., Roberts, J. M., Hall, S. R., Shetter, R. E., Wert, B., Fried, A., Alicke, B., Stutz, J., Young, V. L., White, A. B., and Zamora, R. J.: OH and HO<sub>2</sub> concentrations, sources, and loss rates during the Southern Oxidants Study in Nashville, Tennessee, summer 1999, *J. Geophys. Res.*, 108, 4617, doi:10.1029/2003JD003551, 2003.
- McKeen, S. A., Mount, G., Eisele, F., Williams, E., Harder, J., Goldan, P., Kuster, W., Liu, S. C., Baumann, K., Tanner, D., Fried, A., Sewell, S., Cantrell, C., and Shetter, R.: Photochemical modeling of hydroxyl and its relationship to other species during the Tropospheric OH Photochemistry Experiment, *J. Geophys. Res.*, 102, 6467–6493, 1997.
- Mihelcic, D., Holland, F., Hofzumahaus, A., Hoppe, L., Konrad, S., Müsgen, P., Pätz, H.-W., Schäfer, H.-J., Schmitz, T., Volz-Thomas, A., Bächmann, K., Schlomski, S., Platt, U., Geyer, A., Alicke, B., Perner, D., Klüpfel, T., and Moortgat, G. K.: Comparison of measurements and model calculations of OH, HO<sub>2</sub>, and ΣRO<sub>2</sub> and the local ozone production during the BERLIOZ campaign, *J. Geophys. Res.*, 108, 8254, doi:10.1029/2001JD001014, 2003.
- Monks, P. S., Granier, C., Fuzzi, S., Stohl, A., Williams, M., Akimoto, H., Ammani, M., Baklanov, A., Baltensperger, U., Bey,

- I., Blake, N., Blake, R., Carslaw, K., Cooper, O., Dentener, F., Fowler, D., Fragkou, E., Frost, G., Generoso, S., Ginoux, P., Grewe, V., and H. C. Hansson, A. G., Henne, S., Hjorth, J., Hofzumahaus, A., Huntrieser, H., Isaksen, I. S. A., Jenkin, M. E., Kaiser, J., Kanakidou, M., Klimont, Z., Kulmala, M., Laj, P., Lawrence, M., Lee, J., Lioussé, C., Maione, M., McFiggans, G., Metzger, A., Mieville, A., Moussiopoulos, N., Orlando, J., O'Dowd, C., Palmer, P., Parrish, D., Petzold, A., Platt, U., Pöschl, U., Prévôt, A. S. H., Reeves, C. E., Reimann, S., Rudich, Y., Sellegri, K., Steinbrecher, R., Simpson, D., ten Brink, H., Theloke, J., van der Werf, G. R., Vautard, R., Vestreng, V., Vlachokostas, C., and von Glasow, R.: Atmospheric Composition Change – Global and Regional Air Quality, *Atmos. Environ.*, 43, 5268–5350, 2009.
- Nehr, S., Bohn, B., Fuchs, H., and Hofzumahaus, A.: HO<sub>2</sub> formation from the OH + benzene reaction in the presence of O<sub>2</sub>, *Phys. Chem. Chem. Phys.*, 13, 10699–10708, doi:10.1039/C1CP20334G, 2011.
- Paulot, F., Crouse, J. D., Kjaergaard, H. G., Kroll, J. H., Seinfeld, J. H., and Wennberg, P. O.: Isoprene photooxidation: new insights into the production of acids and organic nitrates, *Atmos. Chem. Phys.*, 9, 1479–1501, doi:10.5194/acp-9-1479-2009, 2009.
- Peeters, J. and Müller, J.-F.: HO<sub>x</sub> radical regeneration in isoprene oxidation via peroxy radical isomerisations. II: experimental evidence and global impact, *Phys. Chem. Chem. Phys.*, 12, 14227–14235, doi:10.1039/c0cp00811g, 2010.
- Peeters, J., Nguyen, T. L., and Vereecken, L.: HO<sub>x</sub> radical regeneration in the oxidation of isoprene, *Phys. Chem. Chem. Phys.*, 11, 5935–5939, 2009.
- Platt, U., Alicke, B., Dubois, R., Geyer, A., Hofzumahaus, A., Holland, F., Martinez, M., Mihelcic, D., Klüpfel, T., Lohrmann, B., Pätz, W., Perner, D., Rohrer, F., Schäfer, J., and Stutz, J.: Free radicals and fast photochemistry during BERLIOZ, *J. Atmos. Chem.*, 42, 359–394, 2002.
- Poppe, D., Wallasch, M., and Zimmermann, J.: The Dependence of the Concentration of OH on its Precursors under Moderately Polluted Conditions: A Model Study, *J. Atmos. Chem.*, 16, 61–78, 1993.
- Poppe, D., Zimmermann, J., and Dorn, H. P.: Field Data and Model Calculations for the Hydroxyl Radical, *J. Atmos. Sci.*, 52, 3402–3407, 1995.
- Pöschl, U., von Kuhlmann, R., Poisson, N., and Crutzen, P. J.: Development and intercomparison of condensed isoprene oxidation mechanisms for global atmospheric modeling, *J. Atmos. Chem.*, 37, 29–52, 2000.
- Pugh, T. A. M., MacKenzie, A. R., Hewitt, C. N., Langford, B., Edwards, P. M., Furneaux, K. L., Heard, D. E., Hopkins, J. R., Jones, C. E., Karunaharan, A., Lee, J., Mills, G., Misztal, P., Moller, S., Monks, P. S., and Whalley, L. K.: Simulating atmospheric composition over a South-East Asian tropical rainforest: performance of a chemistry box model, *Atmos. Chem. Phys.*, 10, 279–298, doi:10.5194/acp-10-279-2010, 2010.
- Read, K. A., Mahajan, A. S., Carpenter, L. J., Evans, M. J., Faria, B. V. E., Heard, D. E., Hopkins, J. R., Lee, J. D., Moller, S. J., Lewis, A. C., Mendes, L., McQuaid, J. B., Oetjen, H., Saiz-Lopez, A., Pilling, M. J., and Plane, J. M. C.: Extensive halogen-mediated ozone destruction over the tropical Atlantic Ocean, *Nature*, 453, 1232–1235, 2008.
- Ren, X., Harder, H., Martinez, M., Leshner, R. L., Oligier, A., Shirley, T., Adams, J., Simpas, J. B., and Brune, W. H.: HO<sub>x</sub> concentrations and OH reactivity observations in New York City during PMTACS-NY2001, *Atmos. Environ.*, 37, 3627–3637, 2003.
- Ren, X., Harder, H., Martinez, M., Faloon, I. C., Tan, D., Leshner, R. L., Di Carlo, P., Simpas, J. B., and Brune, W. H.: Interference Testing for Atmospheric HO<sub>x</sub> Measurements by Laser-induced Fluorescence, *J. Atmos. Chem.*, 47, 169–190, 2004.
- Ren, X., Olson, J. R., Crawford, J. H., Brune, W. H., Mao, J., Long, R. B., Chen, G., Avery, M. A., Sachse, G. W., Barrick, J. D., Diskin, G. S., Huey, L. G., Fried, A., Cohen, R. C., Heikes, B., Wennberg, P., Singh, H. B., Richard, D. R. B., and Shetter, E.: HO<sub>x</sub> Chemistry during INTEX-A 2004: Observation, Model Calculations and comparison with previous studies, *J. Geophys. Res.*, 113, D05310, doi:10.1029/2007JD009166, 2008.
- Ren, X. R., Edwards, G. D., Cantrell, C. A., Leshner, R. L., Metcalf, A. R., Shirley, T., and Brune, W. H.: Intercomparison of peroxy radical measurements at a rural site using laser-induced fluorescence and Peroxy Radical Chemical Ionization Mass Spectrometer (PerCIMS) techniques, *J. Geophys. Res.*, 108, D194605, doi:10.1029/2003JD003644, 2003.
- Rohrer, F. and Berresheim, H.: Strong correlation between levels of tropospheric hydroxyl radicals and solar ultraviolet radiation, *Nature*, 442, 184–187, 2006.
- Rose, D., Nowak, A., Achtert, P., Wiedensohler, A., Hu, M., Shao, M., Zhang, Y., Andreae, M. O., and Pöschl, U.: Cloud condensation nuclei in polluted air and biomass burning smoke near the mega-city Guangzhou, China – Part 1: Size-resolved measurements and implications for the modeling of aerosol particle hygroscopicity and CCN activity, *Atmos. Chem. Phys.*, 10, 3365–3383, doi:10.5194/acp-10-3365-2010, 2010.
- Saiz-Lopez, A., Plane, J. M. C., Mahajan, A. S., Anderson, P. S., Bauguitte, S. J.-B., Jones, A. E., Roscoe, H. K., Salmon, R. A., Bloss, W. J., Lee, J. D., and Heard, D. E.: On the vertical distribution of boundary layer halogens over coastal Antarctica: implications for O<sub>3</sub>, HO<sub>x</sub>, NO<sub>x</sub> and the Hg lifetime, *Atmos. Chem. Phys.*, 8, 887–900, doi:10.5194/acp-8-887-2008, 2008.
- Saunders, S. M., Jenkin, M. E., Derwent, R. G., and Pilling, M. J.: Protocol for the development of the Master Chemical Mechanism, MCM v3 (Part A): tropospheric degradation of non-aromatic volatile organic compounds, *Atmos. Chem. Phys.*, 3, 161–180, doi:10.5194/acp-3-161-2003, 2003.
- Schlosser, E., Bohn, B., Brauers, T., Dorn, H., Fuchs, H., Häsel, R., Hofzumahaus, A., Holland, F., Rohrer, F., Rupp, L. O., Siese, M., Tillmann, R., and Wahner, A.: Intercomparison of Two Hydroxyl Radical Measurement Techniques at the Atmosphere Simulation Chamber SAPHIR, *J. Atmos. Chem.*, 56, 187–205, doi:10.1007/s10874-006-9049-3, 2006.
- Schlosser, E., Brauers, T., Dorn, H.-P., Fuchs, H., Häsel, R., Hofzumahaus, A., Holland, F., Wahner, A., Kanaya, Y., Kajii, Y., Miyamoto, K., Nishida, S., Watanabe, K., Yoshino, A., Kubistin, D., Martinez, M., Rudolf, M., Harder, H., Berresheim, H., Elste, T., Plass-Dülmer, C., Stange, G., and Schurath, U.: Technical Note: Formal blind intercomparison of OH measurements: results from the international campaign HO<sub>x</sub>Comp, *Atmos. Chem. Phys.*, 9, 7923–7948, doi:10.5194/acp-9-7923-2009, 2009.
- Shao, M., Lu, S., Liu, Y., Xie, X., Chang, C., Huang, S., and Chen, Z.: Volatile organic compounds measured in summer in Beijing

- and their role in ground-level ozone formation, *J. Geophys. Res.*, 114, D00G06, doi:10.1029/2008JD010863, 2009.
- Shirley, T. R., Brune, W. H., Ren, X., Mao, J., Leshner, R., Cardenas, B., Volkamer, R., Molina, L. T., Molina, M. J., Lamb, B., Velasco, E., Jobson, T., and Alexander, M.: Atmospheric oxidation in the Mexico City Metropolitan Area (MCMA) during April 2003, *Atmos. Chem. Phys.*, 6, 2753–2765, doi:10.5194/acp-6-2753-2006, 2006.
- Smith, S. C., Lee, J. D., Bloss, W. J., Johnson, G. P., Ingham, T., and Heard, D. E.: Concentrations of OH and HO<sub>2</sub> radicals during NAMBLEX: measurements and steady state analysis, *Atmos. Chem. Phys.*, 6, 1435–1453, doi:10.5194/acp-6-1435-2006, 2006.
- Sommariva, R., Bloss, W. J., Brough, N., Carslaw, N., Flynn, M., Haggerstone, A.-L., Heard, D. E., Hopkins, J. R., Lee, J. D., Lewis, A. C., McFiggans, G., Monks, P. S., Penkett, S. A., Pilling, M. J., Plane, J. M. C., Read, K. A., Saiz-Lopez, A., Rickard, A. R., and Williams, P. I.: OH and HO<sub>2</sub> chemistry during NAMBLEX: roles of oxygenates, halogen oxides and heterogeneous uptake, *Atmos. Chem. Phys.*, 6, 1135–1153, doi:10.5194/acp-6-1135-2006, 2006.
- Stavrakou, T., Peeters, J., and Müller, J.-F.: Improved global modelling of HO<sub>x</sub> recycling in isoprene oxidation: evaluation against the GABRIEL and INTEX-A aircraft campaign measurements, *Atmos. Chem. Phys.*, 10, 9863–9878, doi:10.5194/acp-10-9863-2010, 2010.
- Steiner, A. L., Cohen, R. C., Harley, R. A., Tonse, S., Millet, D. B., Schade, G. W., and Goldstein, A. H.: VOC reactivity in central California: comparing an air quality model to ground-based measurements, *Atmos. Chem. Phys.*, 8, 351–368, doi:10.5194/acp-8-351-2008, 2008.
- Stevens, P. S., Mather, J. H., and Brune, W. H.: Measurement of tropospheric OH and HO<sub>2</sub> by laser-induced fluorescence at low pressure, *J. Geophys. Res.*, 99, 3543–3557, 1994.
- Stevens, P. S., Mather, J. H., Brune, W. H., Eisele, F., Tanner, D., Jefferson, A., Cantrell, C., Shetter, R., Sewall, S., Fried, A., Henry, B., Williams, E., Baumann, K., Goldan, P., and Kuster, W.: HO<sub>2</sub>/OH and RO<sub>2</sub>/HO<sub>2</sub> ratios during the Tropospheric OH Photochemistry Experiment: Measurement and theory, *J. Geophys. Res.*, 102, 6379–6391, 1997.
- Stockwell, W. R., Kirchner, F., Kuhn, M., and Seefeld, S.: A new mechanism for regional atmospheric chemistry modeling, *J. Geophys. Res.*, 102, 25847–25879, 1997.
- Taketani, F., Kanaya, Y., and Akimoto, H.: Heterogeneous loss of HO<sub>2</sub> by KCl, synthetic sea salt, and natural seawater aerosol particles, *Atmos. Environ.*, 43, 1660–1665, 2009.
- Taketani, F., Kanaya, Y., and Akimoto, H.: Kinetics of HO<sub>2</sub> Uptake in Levoglucosan and Polystyrene Latex Particles, *J. Phys. Chem. Lett.*, 1, 1701–1704, 2010.
- Tan, D., Faloon, I., Simpas, J. B., Brune, W., and Shepson, P. B.: HO<sub>x</sub> budgets in a deciduous forest: Results from the PROPHET summer 1998 campaign, *J. Geophys. Res.*, 106, 24407–24427, 2001.
- Taraborrelli, D., Lawrence, M. G., Butler, T. M., Sander, R., and Lelieveld, J.: Mainz Isoprene Mechanism 2 (MIM2): an isoprene oxidation mechanism for regional and global atmospheric modelling, *Atmos. Chem. Phys.*, 9, 2751–2777, doi:10.5194/acp-9-2751-2009, 2009.
- Tas, E., Peleg, M., Matveev, V., Zingler, J., and Luria, M.: Frequency and extent of bromine oxide formation over the Dead Sea, *J. Geophys. Res.*, 110, D11304, doi:10.1029/2004JD005665, 2005.
- Thornton, J. and Abbatt, J. P. D.: Measurements of HO<sub>2</sub> uptake to aqueous aerosol: Mass accommodation coefficients and net reactive loss, *J. Geophys. Res.*, 110, D08309, doi:10.1029/2004JD005402, 2005.
- Thornton, J. A., Woolridge, P. J., Cohen, R. C., Martinez, M., Harder, H., Brune, W. H., Williams, E. J., Roberts, J. M., Fehsenfeld, F. C., Hall, S. R., Shetter, R. E., Wert, B. P., and Fried, A.: Ozone production rates as a function of NO<sub>x</sub> abundances and HO<sub>x</sub> production rates in the Nashville urban plume, *J. Geophys. Res.*, 107, D124146, doi:10.1029/2001JD000932, 2002.
- Volkamer, R., San Martini, F., Molina, L. T., Salcedo, D., Jimenez, J. L., and Molina, M. J.: A missing sink for gas-phase glyoxal in Mexico City: Formation of secondary organic aerosols, *Geophys. Res. Lett.*, 34, L19807, doi:10.1029/2007GL030752, 2007.
- Weinstock, B., Niki, H., and Chang, T. Y.: Chemical Factors Affecting the Hydroxyl Radical Concentration in the Troposphere, *Adv. Environ. Sci. Technol.*, 10, 221–258, 1980.
- Whalley, L. K., Edwards, P. M., Furneaux, K. L., Goddard, A., Ingham, T., Evans, M. J., Stone, D., Hopkins, J. R., Jones, C. E., Karunaharan, A., Lee, J. D., Lewis, A. C., Monks, P. S., Moller, S. J., and Heard, D. E.: Quantifying the magnitude of a missing hydroxyl radical source in a tropical rainforest, *Atmos. Chem. Phys.*, 11, 7223–7233, doi:10.5194/acp-11-7223-2011, 2011.
- Yoshino, A., Sadanaga, Y., Watanabe, K., Kato, S., Miyakawa, Y., Matsumoto, J., and Kajii, Y.: Measurement of total OH reactivity by laser-induced pump and probe technique – comprehensive observations in the urban atmosphere of Tokyo, *Atmos. Environ.*, 40, 7869–7881, 2006.
- Yue, D. L., Hu, M., Wu, Z. J., Guo, S., Wen, M. T., Nowak, A., Wehner, B., Wiedensohler, A., Takegawa, N., Kondo, Y., Wang, X. S., Li, Y. P., Zeng, L. M., and Zhang, Y. H.: Variation of particle number size distributions and chemical compositions at the urban and downwind regional sites in the Pearl River Delta during summertime pollution episodes, *Atmos. Chem. Phys.*, 10, 9431–9439, doi:10.5194/acp-10-9431-2010, 2010.
- Zhang, Y. H., Hu, M., Zhong, L. J., Wiedensohler, A., Liu, S. C., Andreae, M. O., Wang, W., and Fan, S. J.: Regional Integrated Experiments on Air Quality over Pearl River Delta 2004 (PRIDE-PRD2004): Overview, *Atmos. Environ.*, 42, 6157–6173, 2008.
- Zhang, Y. H., Hu, M., Shao, M., Brauers, T., Chang, C. C., Hofzumahaus, A., Holland, F., Li, X., Lu, K., Kita, K., Kondo, Y., Nowak, A., Pöschl, U., Rohrer, F., Zeng, L., Wiedensohler, A., and Wahner, A.: Continuous efforts to investigate regional air pollution in the Pearl River Delta, China: PRiDe PRD2006 campaign, *Atmos. Chem. Phys. Discuss.*, in preparation, 2012.